LONDON, METEOROLOGICAL OFFICE.

Met.O.15 Internal Report No.13.

Thunderstorm electrification in a three dimensional numerical model.By RAWLINS,F.

London,Met.Off.,Met.O.15 Intern.Rep.No.13, 1980,31cm.Pp.32,App.8, 21 pls.19 Refs.

METEOROLOGICAL OFFICE
London Road, Bracknell, Berks.

MET.O.15 INTERNAL REPORT

No 13

THUNDERSTORM ELECTRIFICATION IN A THREE DIMENSIONAL NUMERICAL MODEL

by

F Rawlins

JANUARY 1980

Cloud Physics Branch (Met.O.15)

AM

1. INTRODUCTION

The principal objective of this research is to simulate the generation and distribution of electric charge in a three-dimensional model of a thunderstorm incorporating the ice phase. The sensitivity of the results to various electrical parametrizations can be tested and the effect of different microphysical assumptions explored. This presupposes that a) sufficient qualitative information concerning the electrical behaviour of a thunderstorm is available in order to distinguish realistic results from the merely plausible and that b) the implicit assumptions of the model basis allows an adequate description of the electrical interactions. Both these suppositions will be considered later. Providing that a satisfactory representation can be obtained, the gross characteristics of different charging mechanisms can be examined.

Early attempts to simulate thunderstorm electrification, with electric field strengths sufficient for lightning to occur, utilized models with simple dynamics and a crude calculation of electric field strength, such as in the infinite parallel plate approximation. Some of these models incorporated detailed microphysical calculations, such as in Scott and Levin (1974). More recent papers (Illingworth and Latham (1977), Chiu (1978)) have taken account of the finite cloud size at the expense of discarding some of the microphysical complexity. All these models were axisymmetric. The present model follows this trend, containing a fully three-dimensional non-axisymmetric description of a glaciated cumulonimbus together with a simple parametrization of microscale electrical effects.

Initially effort has been concentrated on the inductive electric growth mechanism in which ice particles collide with hail pellets which are polarized in an external field. The basic dynamical and electrical modelling is described in the next two sections. In order to investigate the effect of some inherent limitations, such as the finite grid size, a simple axisymmetric model was also formulated and is described in Appendix 1. This allowed the rapid testing of a number of the less accessible assumptions included in the scheme.

2. CLOUD MODEL

For a full description of the dynamical model the reader is referred to Miller and Pearce (1974). This is a non-hydrostatic primitive equation scheme with pressure as the vertical co-ordinate. The domain is 16 km x 16 km x 950 mb with horizontal and vertical grid spacings of 1 km and 50 mb respectively and a time step Δt of 15 seconds. The model is used to study the dynamical response of a cumulonimbus to a variety of conditions so that a wide range of ambient wind and thermodynamic fields can be specified. It is assumed for this purpose that, for large scale convection, advective processes dominate the turbulent effects - hence there is a coarse grid and only a simple representation of mixing and diffusion.

The microphysical representation of moist processes follows Kessler (1969) and includes water vapour, cloud water and rain as model variables. The processes described are: the autoconversion of cloud water to rain, the accretion of cloud water by rain and the evaporation of rain. Supersaturated water vapour is assumed to be instantly condensed.

The ice phase parametrization is fully described in Bennetts and Rawlins (——). Briefly, the scheme is similar to that of Wisner, Orville and Meyers (1972), carrying hail (radius 300 μm) and three size classes of ice (radius 0-100, 100-200, 200-300 μm) as model variables. The ice phase is initiated by the activation of ice nuclei, assumed to be already in supercooled

cloud drops, following the Fletcher (1962) expression

$$N_{\mathcal{L}} = 10^{-2} \exp(-0.6T) \qquad (2.1)$$

where $N_{\mathcal{L}}$ is the number of ice nuclei activated per m^3 and T is the temperature in degrees C.

Ice phase calculations include the accretion of cloud water by hail, the freezing of rain by accretion of cloud ice, the accretion of cloud water by cloud ice, the melting of hail, the sublimation of water vapour by ice particles and the resultant transfer between the ice size classes. Contact nucleation is not included and splintering is neglected although the effect of any extra freezing thereby produced can be partly accounted for in the specification of the ice activation expression (2.1).

Hence bulk quantities of rain, hail, ice, cloud water and water vapour are calculated and can be specified for each grid volume. The microphysical scheme was chosen and developed to be suitable for mid-latitude convection, allowing the correct distribution of heat sources and sinks throughout the cloud evolution. To this end comparisons were made with observed clouds in which the regions of precipitation were known from radar studies. It is to be stressed that the emphasis of the model is towards the large scale structure, which then offers a constraint to the microphysical parametrization. Providing that this constraint is met, a number of different assumptions can be made which cannot be distinguished by the model results.

3. ELECTRICAL PARAMETRIZATION

It is assumed that charge separation occurs by the differential advection of charge carrying hydrometeors. Accordingly two charge distributions Q^c and Q^p are specified: the former being the total positive charge residing on cloud particles and the latter being the total positive charge carried by precipitation particles. Hence Q^c is assumed to follow the internal cloud motions alone whereas Q^p will also have some representative group fallspeed.

The electric field $\underline{E}$ is calculated throughout the cloud by solving Poisson's equation for the electrostatic potential ϕ :

$$\Delta^2 \phi = -\frac{(Q^c + Q^p)}{\varepsilon_0 \tau_v} \qquad (3.1)$$

where τ_v is the grid volume.

Then,

$$\underline{E} = -\text{grad}\,\phi \qquad (3.2)$$

Under normal atmospheric conditions the conductivity of the air (at sea level) is $\sigma \sim 2.10^{-14}$ ohm^{-1} m^{-1} with a charge decay time constant of $\tau_d = \frac{\varepsilon_0}{\sigma} \sim 450$ seconds which is large compared to Δt . In the cloud interior the conductivity is probably several orders of magnitude lower, due to the small ions (whose transport forms the conduction current) being collected on cloud drops of low ionic mobility. This justifies the electrostatic approximation and the neglect of

leakage currents within the cloud, except possibly in the proximity of very high electric fields. However the conductivity gradient across a cloud boundary will itself produce a space charge accumulation in the presence of an external electric field. This effect is important for weakly electrified clouds but is ignored in the present case.

The inversion of Poisson's equation was performed by implementing a two dimensional Fourier synthesis in the horizontal directions and a Gaussian elimination method for the vertical co-ordinate. In the early stages of this research some problems were encountered with the boundary values, which were assumed fixed during an integration period in this procedure, since ϕ falls off relatively slowly with distance from a single charge or dipole. This was resolved by evaluating a charge total Q_T for each level at a weighted position $\underline{S}_T$ and calculating the boundary values at $\underline{s}_b$ explicitly through the Gaussian relation:

$$\phi(\underline{S}_b) = \frac{Q_T}{4\pi\varepsilon_0 |\underline{S}_b - \underline{S}_T|} \qquad (3.3)$$

Contributions from Q^{ϵ} and Q^{p} were summed separately since their respective charge centre positions could differ considerably. This allowed an accuracy of about 10% for the few largest fields and considerably better for regions away from the main charge as compared to the very time consuming, completely explicit Gauss calculation.

The greater part of the evidence concerning thunderstorm electrification suggests that the production of strong electric fields is associated with the presence of the ice phase together with precipitation. It has therefore been considered that a principal method of charge generation is by the interaction of ice and hail. A number of mechanisms have been proposed and one seen as likely to account for the high growth rate of the electric field is the inductive electrification of hail as described in Mason (1971). In this process ice particles rebound from the underside of a falling hail pellet which is polarized in the external field. If the external electric field vector is pointed downwards, i.e. in the direction of the fair weather field, the ice crystals remove positive charge leaving the hail particle negatively charged.

The rate of charge generation for a single hail particle of radius r can be represented (in M.K.S.):

$$\frac{dq}{dt} = \frac{1}{\tau}\left(12\pi\varepsilon_0 r^2 \cos\theta E - q\right) \qquad (3.4)$$

where q is the negative charge carried by the hail particle. θ is the angle between the line joining hail and ice particle centres and the hail velocity $\underline{V}$. E is the electric field strength in the direction of $\underline{V}$ and

$$1/\tau = \frac{\pi^3}{6} V e_1 e_2 r_{ice}^2 N_{ice} \qquad (3.5)$$

where e_1 is the collision efficiency, e_2 is the rebound probability and N_{ice} is the number of ice particles per unit volume of cloud, with some average radius r_{ice}.

This formula assumes that the hail and ice particles are spherical with $r \gg r_{ice}$; that the ice crystals are originally uncharged and stationary relative to the hail and that the relaxation time of charge transfer is small compared to the time of contact. The validity of all these assumptions has been challenged.

The approximation $e_1 = 1.0$ is used for the ice/hail collision efficiency in the absence of quantitative data. For water drops in an electric field the hydrodynamic flow may be quite complicated (Wang et al (1979)) and e_1 is generally a function of r and r_{ice}. However from (3.4) and (3.5) it can be seen that the most effective ice crystals for charge transfer are those of large radius and these are more likely to have collision efficiencies approaching unity. The rebound probability is assumed to be $e_2 = 1.0$ although this is certainly not true for the larger hail particles under wet growth conditions when the surface water film will tend to capture incident ice crystals. Large hail will also be of increasingly non-spherical shape, as material is accreted onto the undersides of the particles.

If an ice crystal undergoes multiple collisions with hail the charge transfer mechanism will be inhibited. Equation (3.4) then becomes

$$\frac{dq}{dt} = \frac{1}{\tau}\left(12\pi\varepsilon_0 r^2 \cos\theta E - q - \frac{6r^2}{\pi^2 r_{ice}^2} q_{ice}\right) \quad (3.6)$$

where q_{ice} is the average positive charge residing on an ice particle. However, providing that $\frac{6}{\pi^2}\frac{N r^2}{N_{ice} r_{ice}^2}$ is small, where N is the concentration of hail particles,

the last term can be neglected. This is not a good approximation for the smallest hail pellets.

The relaxation time for charge transfer from hail to ice is $\frac{\varepsilon_0}{\sigma_{ice}} \sim 10^{-2}$ seconds whereas the time of contact is of order $\frac{r_{ice}}{v} \sim 10^{-3}$ seconds for large fallspeeds. This constitutes a limitation to the size of hail for which charge transfer is efficient. Takahashi (1978), in measurements involving a rotating riming surface, gave a threshold collision speed of 7 ms^{-1} which corresponds to a hail radius of about 1 mm.

In order to parametrize the total charge generation the spectrum of hail size was assumed to follow a Marshall-Palmer distribution with the number of hail particles/unit volume/unit radius given by

$$N(r) = 2\, No \exp(-r/rm)$$

where No is a constant. (Compare with the usual notation $N(D) = No \exp(-LD)$). The characteristic radius rm is defined by the volume density of hail ρ_h i.e. the mass of hail/unit volume of air.

$$\rho_h = \int_0^\infty 4/3\, \pi r^3 \rho_{ice} N(r) dr \qquad (3.7)$$

$$= 16\pi \rho_{ice} r_m^4 N_0$$

where ρ_{ice} is the density of ice.

Integrating the charge over all hail sizes and over the grid volume we obtain

$$Q = -\int_0^\infty q N(r) dr \forall_v$$

since r $\lesssim$ 300 microns contributes very little to the integral).

Then from (3.4)

$$\frac{dQ}{dt} = \frac{-1}{\tau}\left(12\pi\varepsilon_0\cos\theta E\int_0^\infty r^2 N(r)\,dr\,\tau_v + Q\right)$$

$$-\frac{dQ^c}{dt} = \frac{dQ^p}{dt} = \frac{-1}{\tau}\left(C_2 E + Q^p\right) \qquad (3.8)$$

$$C_2 = 24\pi\varepsilon_0\overline{\cos\theta}\,N_0\,l_m^3\,\Gamma(3)\,\tau_v$$

$$= \frac{48\pi\varepsilon_0\overline{\cos\theta}\,N_0^{0.25}\,\tau_v\,\rho_x^{0.75}}{(16\pi\rho_{ice})^{0.75}} = 7.72\times10^{-12}\,\tau_v\rho_x^{0.75}$$

Since τ may be of comparable order to the timestep Δt we consider (3.8) over this time.

$$\left(\frac{d}{dt}+\frac{1}{\tau}\right)Q = -\frac{C_2 E}{\tau}$$

$$\int_0^{\Delta t} e^{+t/\tau}\left(\frac{d}{dt}+\frac{1}{\tau}\right)Q\,dt = -\int_0^{\Delta t} e^{+t/\tau}\frac{C_2 E}{\tau}\,dt$$

$$Q e^{+t/\tau}\Big|_0^{\Delta t} = -C_2 E\, e^{+t/\tau}\Big|_0^{\Delta t}$$

providing that C_2 and E are assumed constant during the timestep. This is a reasonable assumption for atmospheric growth rates.

$$Q_{\Delta t} e^{\Delta t/\tau} - Q_0 = -C_2 E\left(e^{\Delta t/\tau} - 1\right)$$

$$\Delta Q = Q_{\Delta t} - Q_0 = -\left(C_2 E + Q_0\right)\left(e^{\Delta t/\tau} - 1\right) \qquad (3.9)$$

and in the model $Q^p = Q^p + \Delta Q$, $Q^c = Q^c - \Delta Q$ where

$$\Delta Q = -(c_2 E + Q^p)(e^{\Delta t/\tau} - 1)$$

to represent the charge generation.

Differential advection then creates a charge separation the hail falling with a group velocity V where

$$V = \frac{\int \frac{4}{3}\pi r^3 v(r) N(r) dr}{\int \frac{4}{3}\pi r^3 N(r) dr} \qquad v(r) \propto r^{1/2} \tag{3.10}$$

$$V \propto I_m^{1/2} \propto \rho_h^{1/8}$$

For a hail pellet falling in equilibrium with an applied electric field we have the balance of forces:

$$\tfrac{1}{2}\pi r^2 C \rho \underline{v}^2(r) = \tfrac{4}{3}\pi r^3 \rho_{ice} g + q(r) E \tag{3.11}$$

where C = 0.6 is a drag coefficient which is approximately constant for large particles.

Let $\underline{v}(r) = \underline{V_0}(r) - \underline{v}^*(r)$

where $\underline{V}^*$ is a retardation velocity and

$$V_0 = \alpha r^{1/2} \rho^{-1/2} \qquad \left(\alpha = 200.0 \text{ kg}^{1/2} \text{ s}^{-1} \text{ m}^{-1}\right)$$

Then $\tfrac{1}{2}\pi r^2 C \rho v^*(r)\left(v(r) + V_0(r)\right) = -q(r)E$

and making the approximation $v(r) + V_0(r) \approx 2 V_0(r)$

$$v^*(r) = \frac{-q(r)E}{\pi r^2 C \rho V_0} \tag{3.12}$$

Taking a mass weighted average of the retardation velocity, by analogy to the undisturbed case (3.10) we have

$$V^* = \frac{\int \frac{4}{3}\pi r^3 v^*(r) N(r)\, dr}{\int \frac{4}{3}\pi r^3 N(r)\, dr}$$

$$V^* = C_3 Q^p E \qquad (3.13)$$

$$C_3 = \left(\frac{16\pi \rho_{ice}}{\rho_a}\right)^{7/8} \left(4\pi C \alpha \rho^{1/2} \tau_v N_o^{1/8}\right)^{-1} \Gamma(7/2)/\Gamma(4)$$

For electric fields much less than for the lightning case $V^* \ll V$.

The values for the constants were initially taken as

$\rho_{ice} = 0.5\ 10^3$ kg m^{-3}

No $= 4.10^4$ m^{-4} (for $r_m \sim 10^{-3}$m, as the maximum in this case, this implies 80 hail particles per m^3).

$\overline{\cos\Theta} = 0.71$

$C = 0.6$

leading to $C_2 = 3.72 \cdot 10^{-3} \rho^{-1} \rho_a^{3/4}$

and $C_3 = 1.35 \cdot 10^{-9} \rho^{1/2} \rho_a^{-7/8}$

For simplicity the starting vertical electric field E_o was assumed constant throughout the cloud with a value of 500 Vm^{-1} and lightning was considered to occur when E $\geq$500 kVm^{-1}. In fair weather the electric field decreases exponentially with height but the initial stages of a cloud, even before precipitation is formed, is likely to show a quite different structure. A real cloud may also be charged initially due to remnants of previous storms in the

same airstream.

In practice two or three electrical timesteps were implemented in every model timestep. Firstly, the electric field was calculated from (3.1) and (3.2), then equations (3.9) and (3.13) were used to determine the charge transfer and velocity retardation. An advection scheme was operated on Q^c and $Q^?$ with the given model velocities, together with the retardation velocity for $Q^?$ only. The hail fallspeed was also adjusted by the fraction V^*/V_c and this constituted the only feedback of electrical processes into the dynamics of the model.

4. RESULTS OF THREE-DIMENSIONAL SIMULATIONS

A winter maritime sounding (an observed case) was used to initiate an ice and hail bearing cloud integration. The cloud grew to 7 km with a width of order 3 km. The adiabatic water content was 4.5 gm kg^{-1} which gave a maximum ice mixing ratio of $\sim$ 1 gm kg^{-1} and a maximum precipitation rate of 30 mm hr^{-1} at the ground, the precipitation continuing for over 30 minutes. The charging zone, i.e. the region of coexistence of hail and ice under our assumptions, was of order 3 km in vertical extent. The observed cloud did not produce lightning.

Advection scheme

The growth of the electric field was found to be partly dependent on the advection scheme used for the movement of charge. This indicates that the numerical method is insufficient to deal with the detail of the positive feedback mechanism. However, conclusions can be drawn concerning the general structure of electrical behaviour and the reasons for the various shortcomings are instructive.

Advection in the basic cloud model is performed using a centre difference formulation with even and odd timesteps giving an unconditionally unstable scheme but with a very small amplification factor. Large smoothing of the advected variables then reduces the instability. In the charge system large gradients are necessary

to produce strong electric fields and so therefore no smoothing was applied in this first attempt of modelling. The scheme preserves the shape of wavenumber disturbances but at the expense of creating spurious upstream negative values. At the level of the charging zone there were strong winds which produced an upstream perturbation and which became manifest as a counter dipole in the charge distribution. The inverted dipole then interferred with the original dipole structure (which enhanced the fair weather field).

It was next attempted to use a scheme which preserves the advected quantity, i.e an upstream method. A simple upstream forward difference method was introduced and was found to produce very smooth fields. Hence the electrical growth rates were greatly retarded whatever other conditions were applied since this scheme is highly damping and does not preserve small scale structure.

A more computationally expensive method was then tried in order to resolve the small scale gradients whilst preserving positive quantities in the advected fields. This was an upstream finite element spline method which has good damping properties for high wavenumbers. This method gave similar results to the centre difference scheme for early stages of growth but with much less spurious upstream advection. Total charge conservation over the cloud as a whole was also improved significantly. This method was therefore preferred for all later work.

Field structure

For a certain range of microphysical assumptions the maximum electric field surpassed the lightning threshold (see next section). Less rapid rates of growth

generally gave the same mode of development however. Initially, once sufficient hail was formed in the up-draught, charge was created in a region at which $T \sim -25^{\circ}C$. As the production and advection of charge progressed a dipole distribution developed with positive charge, associated with ice crystals, in a relatively compact region above the negative charge, associated with hail - see Figure 1 . The position of the maximum field strength became higher in the cloud as hail was taken up in the updraught and field strengths grew at a near exponential rate, see Figure 3 .

However, once field strengths exceeded about 30 kVm^{-1}, the charge structure was noticeably that of a multipole with a reverse field underneath the principal dipole, as in Figure 2 . This reverse field grew and became extended upwards; finally a series of alternating charges was formed. This is in agreement with the results of Illingworth and Latham (1977) for the inductive effect with a narrow axially symmetric cloud, and who also quoted some observational evidence for such field reversals. Chiu (1978), with an inductive model including the water phase only, also simulated a field reversal underneath the main dipole but ascribed this effect to another cause, concerning the flow of charge to the boundary.

The reverse dipole is produced in this case by highly negatively charged graupel falling to a level below the main negative charge. The graupel then transfers negative charge on impact with the colliding ice crystals, since the charge amount exceeds the inductive limit, and strengthens the main negative charge zone until the field reverses in this region. Then the charging down (i.e. charge transfer in the opposite sense to formerly)

proceeds rapidly since now both terms in equation (3.8) are of the same sign and the counter dipole grows strongly.

A simple analytic model indicating how oscillatory modes of development of the type discussed above can occur and the effect of the cloud charging zone dimensions is described in Appendix 2. The present results were further supplemented by a simple axially symmetric scheme, described in Appendix 1. This formulation was used to check the consistency of the numerical methods employed and to examine isolated parameters that were not easily varied in the three dimensional model.

Once a lightning stroke was adjudged to have occurred (with $E > 500 kVm^{-1}$) the charge concentration was reduced everywhere in the model by the same fraction (usually to 30% of the original values). Since the growth rate was near exponential the charge was quickly refurbished and more lightning strokes were produced at intervals of about 2 minutes of cloud time. This is a very crude treatment of the lightning discharge process and is not intended as a serious representation of the many extremal effects of very high thunderstorm electric fields. It does indicate, however, the relative ease of producing multiple flashes in such a rapidly regenerating process.

Microphysical parametrizations

There are large variations in the measurements of ice and graupel size and numbers concentrations in the atmosphere, which allow some latitude in the choice of parametric constants. The ice particle concentrations are a direct

model result and have not been modified. The hail size concentration is assumed to follow a Marshall-Palmer distribution, with the proportion of smaller hail particles being determined by the intercept No, taken as a constant.

Initially No = 4.10^4 m^{-4} was chosen, the value appropriate from measurements of large particles where usually $r > 2$ mm (Federer and Waldvogel (1975); Musil et al.(1976); Waldvogel, Schmid and Federer (1978)), also used by Orville and Kopp (1977) for numerical modelling of a hailstorm. The correct representation of large hail is important for reproducing precipitation rates and latent heat changes since most of the total hail water content is made up of the larger particles. However for the electrical interactions the hail is generally small with a low precipitation rate. Measurements of graupel with $r < 2$ mm, where the greater part of charge transfer is expected to occur, have produced very different estimates, with N_o up to $10^8 m^{-4}$ (Simpson and Wiggert (1971), Harimaya (1978)). With $N_o = 4.10^4 m^{-4}$ little field growth was obtained, whatever other conditions were applied. When $N_o = 4.10^6 m^{-4}$ was used there was sufficient field growth for lightning to occur under the given assumptions of the cloud simulation see Figure 3 .

The Marshall-Palmer representation of the hail spectrum is a time and space average, derived mostly from samples of the larger hail particles, particularly at the surface. There is some evidence that over short periods in the cloud interior the size spectrum is essentially monodispersed (Auer and Marwitz (1972)).

However over the volume of the charging region, perhaps several km^3, and the time of growth ($\sim$ 20 minutes) an exponential distribution will probably be the best estimate. An alternative size spectrum of the form $N(r) = N_o (r_m/r)^3 \exp(-r/r_m)$ allows some compatibility between the various measurements (Auer (1972) also deduced an inverse cubic dependence) and may be examined in the future.

It must be remembered that the model microphysics was developed and refined to account for the large scale precipitation and evolution of some average members in a range of clouds. Therefore only bulk quantities are predicted and elaborate microphysical assumptions cannot be justified within the limitations of the model framework. Providing reasonable approximations are made, however, the model variables are more closely constrained than in some axisymmetric schemes since the cloud evolution as a whole must be considered to be acceptable.

Cloud type

The spatial distribution of ice and hail in the simulation is controlled by the ice phase parametrization, which was originally chosen to give the best agreement with cloud observations i.e. cloud size, growth and regions of precipitation. Changes in the parameters of the microphysical processes were used to investigate the effect on the charging zones.

The ice/hail interaction zone is shown in Figure 5 for the original Fletcher activation dependence $N_a = 10^{-2} \exp(-0.6T)$ crystals m^{-3}. The effective

forcing in equation (3.8) is given by $N_{ice} \Gamma_{ice}^2 \frac{\rho_h^{.625}}{\rho^{1/2}}$ and this is indicated in the figure. It can be seen that the vertical extent of the charging zone is relatively narrow and that the large hail concentrations lower in the cloud do not contribute to the electrical growth. Increasing the ice activation to $N_{ice} = 10^{-1} \exp(-0.6T)$ produced more ice at higher temperatures and extended the charging zone - see Figure 6 . However the strength of the ice/hail interaction was generally reduced and the electrical growth rate was smaller than in the previous case. On the other hand a decrease in the ice activation, with $N_{ice} = 10^{-3} \exp(-0.6T)$, gave less hail (see Figure 7) and a narrow charging zone, again reducing the growth rate of the maximum electric field, as indicated for these cases in Figure 4 .

The effect of other parameters can be investigated if required, provided that the constraints of the ice phase representation already indicated are not exceeded. That the simple size and shape of the charging zone are major governing factors for field growth is considered in the Appendices.

Shear

In the case under consideration these was a relatively strong shear, 8 ms^{-1} over the charging layer which produced a marked inclination of the main dipole. Clearly this reduces the vertical field strength for a given charge separation. When the effect of shear was removed from the electrical parametrization only, i.e. the horizontal velocities of the charge distributions

were adjusted, the rate of electric field growth doubled in about 8 minutes. However when the ambient wind field of the model as a whole was amended to nullify the upper level shear it was found that the electric field actually grew more slowly than in the undisturbedcase. This appeared to be due to a reduction in the duration of precipitation.

Thus it seems probable that some optimum degree of shear will produce the maximum field growth for this type of cloud with a balance between separation of updraught and downdraught for long lived precipitation and the proximity of charge centres of opposite sign. This is an area of research that could be pursued in the future.

5. DISCUSSION

Early calculations using a parallel plate significantly overestimate the electric field strength. Axisymmetric models take account of the finite lateral spread of charge but will still, in general, produce vertical electric fields that are too large (for the quantity of charge separated). This is because such models assume an optimum distribution, with charge aligned along the vertical which will not be the case in a cloud with shear. Also the effect of lateral variations in the electric field are not necessarily included. Processes which involve a positive feedback mechanism, such as in the inductive method, are very sensitive to field overestimates especially with the degree of uniformity imposed by the condition of axisymmetry. Therefore a local calculation of field strength through the electrostatic potential is less likely to produce systematically high values. In fact, the inversion of Poissons equation in the present scheme will smooth out the charge distribution if the model grid separation is not sufficiently small.

Other models of electric field growth have allowed a greater flexibility in changing the large scale electrical parameters in order to obtain rapid growth but have strong constraints on their microphysical behaviour. This model imposes limitations on the permitted charge distributions but at the expense of the accuracy of the microphysical representation. The sum of such schemes, however, enables a more closely defined range of possible solutions for comparison with observations.

The simplicity of the ice phase representation requires the estimates of hail and ice concentrations to be regarded as very approximate but capable of imposing limitations on arbitrarily specified thunderstorms. The effect of the omission of splintering, wet hail growth and contact nucleation from the model is not known, but all would be expected to have more influence at rather warmer temperatures than obtain in the main regions of charge generation in this model.

For comparative purposes it was thought desirable to decouple the microphysical and electrical assumptions in the formulation of electric field growth. The microphysical requirements for reproducing the large scale dynamics are that the latent heat charges and distribution of water substance should be adequately treated. In order to account for electrical effects, however, the size dependent interactions of various particles must be correctly described, a much more difficult problem. Major changes in the microphysical characteristics influencing electrical behaviour may have little effect on the cloud dynamics. This is not be to confused with feedback of the electric field into the dynamics via the retardation of falling hail which is the only link the model allows. This is a separate problem which may be elucidated in the future, given the terms of reference of this model.

It has been stressed that the connection between the large scale precipitation, which is accessible to the modelling effort, and the electrical interactions, for which little definite information is available, is not direct. From Figure 5 it can be seen that the major charge generation occurs when $\rho_r < 3.10^{-4}$ kg m^{-3} (approximately equivalent to 1 mm hr^{-1}). The maximum precipitation rate

at the ground for this cloud was 30 mm hr^{-1} but it is possible to envisage circumstances for which little growth of the hail would occur so that strong fields could be produced with a low precipitation rate, providing that the circulation was maintained.

In the model rapid electrical growth was possible when N_o was large implying that many small graupel are required which in turn predicts a relatively low ice/hail collision speed. This alleviates one of the major assumptions, that the ice/hail contact time is sufficient for full charge transference. However the assumption that ice crystals are initially uncharged becomes less probable - the effect of multiple collisions is yet to be investigated.

The major consequence of treating the inductive effect alone concerns the structure of the electric field, which is also examined in the Appendices. Most observations of electrical structure have indicated the simple main dipole, with positive charge above negative, together with a smaller positive charge at approximately the freezing level (e.g. Kuettner (1950)). This differs from the model results, which predicts a more complicated multipole system at high field strengths for the relatively narrow cloud studied. It is intended, if possible, to examine the effect of the cloud being wider in extent when a simpler and more rapid dipole growth is expected.

6. CONCLUSIONS

The electrification of a cumulonimbus sufficient for lightning to occur with only the inductive ice/hail generation mechanism can be simulated in a three-dimensional model with the given assumptions, for convenience listed in the latter part of this section. The numerical scheme is considered to be adequate to examine the qualitative effects of charge production through a careful treatment of the advection terms but that a finer grid is required in cases where the charging region is small. A smaller grid is generally expected to produce slightly higher rates of electric field growth. It is to be noted that the deficiencies of advection schemes are usually alleviated by some sort of smoothing operator, perhaps based on a physical process (diffusion) but this has not yet been attempted.

The most sensitive parameter is No, which controls the hail size spectrum in the electrical parametrization only. For rapid electrical growth a large value of N_o is required, commensurate with measurements obtained for samples of small hail or graupel. Thus for electrification by induction tobe favoured there should be a preponderance of small graupel. This is quickly ascertained by an examination of equations (3.4) and (3.7).

An important result obtained for the inductive effect is that the charge structure becomes complicated at high field strengths with the electric vector direction alternating with height for the relatively narrow cloud studied. The cumulative effect of large clouds allows a greater latitude in the descriptions

of the microphysical interactions contributing to the electric charge build up. Thus it should be easier to distinguish the implications of various charging mechanisms in those smaller clouds which only just produce a lightning flash.

Major changes in the activation of ice crystals produced rather smaller changes in the electrical growth rates since it is the interaction zone where ice and hail co-exist which determines the charging process. In this way the position and extent of the charging zone was adjusted rather than the strength of the interaction. In fact a balance of effects was obtained so that there was a maximum field growth rate for a particular ice activation rate. It is interesting that the activation spectrum chosen for a best fit with the observed precipitation distribution also gave the maximum field growth. This is perhaps a consequence of the requirement for a steady and long lived development in both cases.

Further effort is required to examine the effect of vertical wind shear in the charging zone.

A future stage of research is to introduce other postulated electric generation mechanisms which will provide alternative, and hopefully observable, predictions. This study has shown the need for a more complete representation of the ice phase in regard to those processes contributing to the electrical effects and this may be even more important in other processes. For instance very large values of ice content do not lead to excessive electrical growth with the inductive process since a maximum equilibrium charge content is soon reached, as is shown by an inspection of equations (3.5) and (3.9). In an ice-ice process this would be critical however.

There are obvious drawbacks in deriving electrical behaviour from the simulation of a cloud which did not itself produce lightning and for which no electrical measurements were made. It is therefore considered important to obtain a more complete comparison, with some information concerning the electric field growth rate and charge distribution to supplement the necessary thermodynamic description. Microphysical measurements would also aid an assessment of the various assumptions incorporated in the model.

Assumptions in the present electrical scheme

1. Generation of charge is by the inductive hail/ice collision mechanism only; charge separation is by the differential advection of hail with respect to ice; ice crystals are initially uncharged.

2. The stochastic collision process can be represented using bulk values of ice and hail in a coarse grid.

3. The hail size spectrum follows a Marshall-Palmer distribution.

4. The rebound probability and collision efficiency for ice/hail both equal unity.

5. The ice/hail contact time is sufficient to allow a full transference of charge.

6. The average angle of the line joining the hail and ice particle centres is 45°; spherical particles are assumed with $r_{hail} \gg r_{ice}$.

7. The cloud microphysical interactions are unaffected by the electric field except for the direct electrical forces acting on charged hail particles. This

velocity perturbation is assumed small compared with gravity until very high fields are encountered.

8. Boundary effects are unimportant.

9. Melting layer effects are not included.

10. Leakage currents are neglected.

11. The cloud physics variables are considered fixed for the duration of a timestep (15 seconds).

12. The initial vertical electric field is constant at 500 Vm^{-1}; lightning occurs when the field exceeds 500 kVm^{-1}.

7. NOTATION

The following list describes the constants used in the main sections of this paper. The symbols in the Appendices are defined where they are introduced.

$\underline{E}$	Vm^{-1}.	Electric field vector.
$E = \underline{E}.\hat{\underline{v}}$	Vm^{-1}.	Component of electric field in direction of hail velocity.
C		Drag coefficient of hail.
N	m^{-3}.	Number of hail particles per unit volume.
$N(r)$	m^{-4}.	Concentration of hail particles per unit hail radius.
N_a	m^{-3}.	Number of ice nuclei activated per unit volume.
N_{ice}	m^{-3}.	Number of ice particles per unit volume.
N_o	m^{-4}.	Marshall-Palmer hail size distribution intercept.
Q^c	C.	Total charge carried by cloud and ice particles in one grid volume.
Q^p	C.	Total charge carried by precipitation particles in one grid volume.
T	^oC.	Temperature.
e_1		Ice-hail collision efficiency.
e_2		Ice-hail rebound probability.
g	ms^{-2}.	Acceleration due to gravity.
q	C.	Negative charge carried by a single hail pellet.
r	m.	Radius of hail particle.
r_{ice}	m.	Radius (mean) of ice particle.
r_m	m.	Characteristic mean hail radius .
$\underline{v}$	ms^{-1}.	Hail velocity (positive downwards).
$\underline{v}_o$	ms^{-1}.	Hail velocity in the absence of an electric field.
$\underline{v}^* = \underline{v}_o - \underline{v}$	ms^{-1}.	Retardation of hail velocity due to an electric field.
Δt	s.	Model timestep.
ΔQ	C.	Model charge increment.
ε_o	$C^2N^{-1}m^{-2}$.	Permittivity of free space.
ϕ	V.	Electrostatic potential.
θ		Angle between hail velocity vector and the line joining hail and ice particle centres in contact.
ρ	kgm^{-3}.	Density of air.
ρ_{hail}	kgm^{-3}.	Volume density of hail i.e. mass of hail per unit volume air.
ρ_{ice}	kgm^{-3}.	Density of ice.
τ	s.	Ice-hail interaction time constant.
τ_v	m^3.	Model grid volume.

REFERENCES

AUER A.H. 1972 Distribution of graupel and hail with size. Mon.Weather Rev., 100 pp 325-328.

AUER A.H. and MARWITZ J.D. 1972 Hail in the vicinity of organized updraughts. J.Appl.Met., 11 pp 196-198.

BENNETTS D.A. and RAWLINS F. Mid-latitude cumulonimbus convection -- a numerical and observational study. Submitted to Quart.J.R.Met.Soc.

CHIU C.S. 1978 Numerical study of cloud electrification in an axisymmetric, time dependent cloud model. J.Geophysical Res., 83 pp5025-5049.

FEDERER B. and WALDVOGEL A. 1975 Hail and raindrop size distributions from a Swiss multicell storm. J.Appl.Met., 14 pp 91-99.

FLETCHER N.H. 1962 The physics of rainclouds. Cambridge University Press.

HARIMAYA T. 1978 Observations of size distribution of graupel and snowflake. Hokkaido Univ.,Fac.Sci.J., 11 pp 67-77.

ILLINGWORTH A.J. and LATHAM J. 1977 Calculations of electric field growth, field structure and charge distributions in thunderstorms. Quart.J.R.Met.Soc., 103 pp 281-295.

KESSLER E. 1969 On the distribution and continuity of water substance in atmospheric circulation. Met. Monograph, Am.Met.Soc. 10.

KUETTNER J. 1950 The electrical and meteorological conditions inside thunderclouds. J.Met.Am.Met.Soc., 7 pp 322-332.

MASON B.J. 1972 The Bakerian lecture,1971. The physics of the thunderstorm. Proc.R.Soc. A327 pp433-466.

MILLER M.J. and PEARCE R.P. 1974 A three dimensional primitive equation model of cumulonimbus convection. Quart.J.R.Met. Soc., 100 pp 133-154.

MUSIL D.J.,MAY E.L.,SMITH P.L. and SAND W.R. 1976 Structure of an evolving hailstorm.Part IV : Internal structure from penetrating aircraft. Mon.Weather Rev., 104 pp 596-602.

ORVILLE H.D.and KOPP F.J. 1977 Numerical simulation of the life history of a hailstorm. J.Atmos.Sci., 34 pp1596-1618.

SCOTT W.D. and LEVIN Z. 1975 A stochastic electrical model of an infinite cloud : charge generation and precipitation development. J.Atmos.Sci., 32 pp 1814-1828.

SIMPSON J. and WIGGERT V. 1971 1968 Florida cumulus seeding experiment : numerical model results. Mon.Weather Rev. , 99 pp 87-118.

TAKAHASHI T. 1978 Riming electrification as a charge generation mechanism in thunderstorms. J.Atmos.Sci., 35 pp 1536-1548.

WALDVOGEL A.,SCHMID W. and FEDERER B. 1978 The kinetic energy of hailfalls — Part I : hailstone spectra. J.Appl.Met., 17 pp 515-520.

WANG P.K.,GROVER S.N. and PRUPPACHER H.R. 1978 On the effect of electric charges on the scavenging of aerosol particles by clouds and small raindrops. J.Atmos.Sci., 35 pp 1735-1743.

WISNER C.,ORVILLE H.D. and MEYERS C. 1972 A numerical model of a hail bearing cloud. J.Atmos.Sci., 29 pp 1160-1181.

FIGURE CAPTIONS

Fig. 1 The total charge in a horizontal layer, Q^c, Q^p distributions (C) and electric field maxima (kVm^{-1}) against pressure in mb. For this case $N_o = 4.10^6\ m^{-4}$ and t = 32 minutes of cloud time.

Fig. 2 As for (1), except that t = 44 minutes of cloud time.

Fig. 3 The maximum electric field E (kVm^{-1}) as a function of cloud time for different values of N_o.

Fig.4 As for (3), for different values of the Fletcher spectrum $N(T)$, with $N_o = 4.10^6\ m^{-4}$.

Fig. 5 Cloud physical quantities at t = 40 minutes cloud time : the max. hail density ρ_R (kgm^{-3}), ice concentration $\propto$ (radius)^2 nr^2 (m^{-1}) and the forcing term $\rho_R^{0.625} N_{ice} r_{ice}^2 \rho^{-1/2}$ as a function of pressure in mb.; approximate temperatures are also indicated.

Fig. 6 As for (5), with the Fletcher spectrum $N(T) = 10^{-1} \exp(-0.6T)$.

Fig. 7 As for (5), with the Fletcher spectrum $N(T) = 10^{-3} \exp(-0.6T)$.

APPENDIX 1

The three dimensional model is intended to offer a reasonably detailed account of the total cloud evolution and much of the numerical formulations are interrelated in order to obtain a balanced system. The effect of the basic numerical parameters employed are best investigated using a simple model, where the results can be quickly and easily evaluated. Therefore a finite axisymmetric model was constructed similarly to that of Illingworth and Latham(1977).

The model contained N levels of radius R, height z_i, with cloud and precipitation total charges Q_i^c , Q_i^p for each cylindrical slab layer i. The Q^p charges were advected with a constant fallspeed V and the precipitation rate was assumed constant throughout the charging zone. The charging zone was described by an ice/hail interaction time constant τ , which was related to the ice concentation, and was a function of height. The electric field E_i was assumed to be vertical and was calculated directly from

$$E_i = \sum_{j=i+1}^{N} \frac{(Q_j^c + Q_j^p)}{2\pi\varepsilon_0 R^2}\left[1 - \frac{z_{ij}}{\sqrt{R^2 + z_{ij}^2}}\right] + \sum_{j=1}^{i-1} \frac{(Q_j^c + Q_j^p)}{2\pi\varepsilon_0 R^2}\left[-1 - \frac{z_{ij}}{\sqrt{R^2 + z_{ij}^2}}\right] \qquad (A.1)$$

where $z_{ij} = z_j - z_i$

(Note that this expression differs slightly from that of Illingworth and Latham (equation 10)).

This is the vertical field at the centre of each disk and the average field over the disk as a whole will be smaller. Inspection of the field variation for the range of cases considered here has shown this error to be small however.

Then from equation (3.9)

$$-\frac{dQ_i^c}{dt} = \frac{dQ_i^p}{dt} = -\left(e^{\Delta t/\tau} - 1\right)\left(c_2 E_i + Q_i^p\right) \qquad (A.2)$$

where c_2 is taken as a constant throughout the integration

and $$c_2 = a_1 R^2 \Delta z \qquad (A.3)$$

where $\Delta z = z_N/N$ and z_N is fixed at 14 km — which is approximately the three dimensional model height domain.

A default set of constants were chosen as follows :

$N = 40$ giving $\Delta z = 350$m

$R = 2.0$ km

$\Delta t = 7.5$ seconds

$a_1 = 3.0\ 10^{-14}$ (m.k.s. units) which is equivalent to 10^{-3} kg m^{-3} or 36 mm hr^{-1}

$V = 10$ ms^{-1}

and $1/\gamma = 10^{-1}(1.0 - 0.1(z - 9)^2)$ sec^{-1} (z in km) and only positive values are allowed.

The advection procedure was the finite element spline method.

The parameters were varied about these mean values in a number of comparisons described below.

Field growth

The conditions chosen were relatively favourable for growth, although not physically unrealistic, and allowed a near exponential increase in the maximum electric field to values exceeding the lightning threshold within a typical cloud lifetime.

In agreement with results for the three dimensional model a complicated, alternating charge structure was observed, as shown in Figure A.1.

Vertical grid length

The maximum electric field growth rate for various values of Δz is shown in Figure A.4. In the three dimensional model the vertical spacing is of order 0.7 km and this can be seen to slightly underestimate the electrical development. However a limit to the growth curves is obtained for smaller grid spacings, which are still sufficiently large to satisfy the C-F-L criterion in this test. The critical length scale is the charging length $l_c = V\gamma$, i.e. the path length which falling hail require to reach their maximum equilibrium charge. In this example l_c has a minimum value of 75 m but will, in general, be rather larger, commensurate with the more modest fallspeeds and ice concentrations assumed in the main model (e.g. l_c = 400 m for $N_{ice}=10^2$ ice crystals/litre).

The shape of the charge structure was preserved for all choices of Δz, with the positions of field reversals being unchanged, subject to their separation being defined by the grid resolution. As would be expected, the amplitudes of charge and field variations were dampened by the increasing grid size.

Cloud width

The field growth curves for a selection of cloud radii R are shown in Figure A.5, together with the number of field reversals within the charging zone. This clearly indicates the strong dependence of the rate of electrical growth on the cloud width, providing that the assumption is met, that cloud physical interactions are coherent across the horizontal domain.

The charge structures obtained for different radii are shown in Figures A.1, A.2 and A.3 and these demonstrate the increasing complexity of the charge configuration with decreasing cloud width. Another pertinent length scale is l_E, the vertical distance over which the electric field has the same direction. This is a function of both R and a_1, with $l_E \sim 1.5$ km for the standard case, increasing with R. When l_E exceeds some fraction of the total charging zone extent, therefore, the charge configuration will be dominated by a simple dipole.

Time step and advection scheme

Figure A.6 indicates the minimal effect of using a shorter time step in the calculations. This justifies the use of a large time step, providing that the C-F-L condition is satisfied.

The three advection schemes described in the main section are compared in Figure A.7 for the standard case. The earlier conclusions are reinforced by the differing behaviour shown : the centre difference method produces rapid growth but with spurious negative quantities outside the main charging zone; the simple upstream method damps down all the gradients leading to a reduced rate of generation. In the three dimensional model the extra degrees of freedom will exacerbate the problems.

Charging zone

A simple symmetric dependence on height about 9 km was chosen in all cases for the ice crystal concentration, with no ice outside a $\pm$ 3 km range. Figures A.8 and A.9 show the field growth for broad and sharp ice concentration distributions within these limits, and which are to be compared with the default case in Figure A.5. Similar plots are obtained but with the most rapid growth for the broader zone case, as would be expected. It can be noted that the electric field showed fewer changes of direction when the distribution was sharp; the large values of γ outside the very centre of the charging zone restrict the electric charge carried by the hail to well below the maximum equilibrium value.

The results for a weakened interaction zone, i.e. with less ice, are also shown in Figure A.10 for comparison.

Fallspeed

The effect on the electric field growth of varying the fallspeed V is shown in Figure A.11. This indicates that sufficiently rapid rates of charge generation may be obtained providing that a realistic fallspeed is specified.

Discussion

The results listed above indicate that the numerical scheme can treat the positive feedback of the inductive mechanism consistently, although a smaller vertical grid spacing is to be preferred for the present range of parameters. The alternation of field direction with height is also shown to be largely independent of the chosen numerical scheme and that the electrical evolution is broadly similar to that of the three dimensional model.

Two scale lengths , l_c and l_E , are considered important in deciding the nature of the charge structure, together with the actual charging zone dimensions.

An estimate of l_E can be made from the following arguments : consider a cylindrical region of height 2z, radius R with uniform charges +q and -q, separated vertically, each in a volume Rz. From equation (A.2) it can be seen that the maximum charge producee for a vertical field E before discharging occurs is

$$q_{max} = Ea_1 R^2 z \qquad (A.4)$$

From equation(A.1) the field produced by the opposing charge q is

$$E = \frac{q}{2\pi\varepsilon_0}\left[1 - \frac{z}{\sqrt{R^2+z^2}}\right] \qquad (A.5)$$

If $q > q_{max}$ discharging will create a new equilibrium distribution. If $q < q_{max}$ a unidirectional field is allowed and in the limiting case we have $l_E = z$ which gives the vertical distance over which the electrical field is of the same sign, consistent with the attendant charges.

From (A.4) and (A.5) $q = q_{max}$ if $2\pi\varepsilon_0 = a_1 z\left(1 - \frac{z}{\sqrt{R^2+z^2}}\right)$

or $$\frac{z}{1 - \frac{z}{\sqrt{R^2+z^2}}} = \frac{2\pi\varepsilon_0}{a_1} = z_1 \qquad (A.6)$$

where $z_1 \sim 2$ km for the default case and is a function of the microphysical terms, not the cloud scale.

Now for wide clouds $z = l_E \approx Rz_1/(R + z_1) \sim z_1$ and l_E is large, possibly greater than the charging zone extent so that a simple dipole is formed. For R of order z_1 , $z = l_E < z_1$ and an alternating electric field is allowed if l_E is smaller than the vertical cloud charging zone dimension.

Since the equilibrium charge given by (A.4) is not applicable within the finite distance l_c this constitutes a lower limit so that $l_E \geqslant l_c$.

The length scales R, z, z_1, l_E, l_c are, in general, of much the same order in a real cloud and the interplay of effects suggested here will lead to a complex overall behaviour.

APPENDIX 2

This section indicates how an oscillatory electric field can arise with the inductive effect, as discussed previously, instead of the dipole structure usually assumed. This is an elementary analytic treatment, requiring somewhat unrealistic assumptions but it does outline a range of conditions for which the simple dipole configuration can be obtained.

The cloud is assumed to be axisymmetric with charge densities ρ^c, ρ^p with vertical advection of the charge species ρ^- only. Equation (3.8) then becomes

$$\frac{\partial \rho^p}{\partial t} = -\frac{1}{\tau}\left(a_2 E + \rho^p\right) - v\frac{\partial \rho^p}{\partial z} \qquad (A.7)$$

and

$$\frac{\partial \rho^c}{\partial t} = \frac{1}{\tau}\left(a_2 E + \rho^p\right) \qquad (A.8)$$

where E is the downward pointing field strength, v is the (positive) fallspeed, $a_2 = a_1/\pi$ and a_1, τ are defined in section 3. For this analysis a_1, τ, and v are assumed constant throughout the cloud. Poisson's equation for the cylindrical co-ordinates (z,R) becomes

$$\frac{1}{R}\frac{\partial}{\partial R}\left(-RE_R\right) + \frac{\partial E}{\partial z} = -\frac{1}{\varepsilon_0}\left(\rho^c + \rho^p\right) \qquad (A.9)$$

where E_R is the radial electric field.

Consider the small region near the axis of a wide cylindrical cloud. Here E_R and $\frac{\partial}{\partial R}E_R$ will be small, tending to zero for an infinite cloud. We therefore approximate (A.9) by

$$\frac{\partial E}{\partial z} = -\frac{1}{\varepsilon_0}\left(\rho^c + \rho^p\right)\left(1-\alpha\right) \qquad (A.10)$$

where α is a form factor, dependent on the cloud aspect ratio and is taken to be a constant. Then (A.7),(A.8),(A.10) constitute a linear set in ρ^c, ρ^p, E for wave disturbances of the form $\exp i(kz + \sigma t)$. This is strictly valid only for the limit $\alpha \to 0$ corresponding to an infinitely wide cloud.

Combining the harmonic linear set one obtains an eigenvalue relation with allowed solutions providing that :

$$\sigma^2 - \sigma\left(i/\tau + kv\right) + \frac{a_2 v}{\varepsilon_0 \tau}\left(1-\alpha\right) = 0 \qquad (A.11)$$

(Either sign of k leads to the same solution.) We assume τ = 10 seconds, v = 10ms^{-1} $\frac{a_2 V}{\varepsilon_0 r}(1-\alpha)$ = 2.5 10^{-3} s^{-2} as representative values and consider solutions of the form $\sigma = \sigma_r + i\sigma_i$. The time dependence for each species is now $\exp i\sigma_i T . \exp -\sigma_r T$; the growing modes given by a negative σ_r are shown in Figure A.13. In regions of solution space where $|\sigma_i| > |\sigma_r|$ the mode growth will be dominant over the oscillation term and, noting that the fastest growth occurs for the largest length scales, a simple dipole structure will be observed.

Figure A.14 identifies the threshold of vertical length scales L = 2 π /k for which $|\sigma_i| = |\sigma_r|$ as a function of the forcing term $\frac{a_2 V}{\varepsilon_0 r}(1-\alpha)$, and also the limit for which $|\sigma_i| > 6.10^{-3}$ sec^{-1} , which is the required rate of growth for lightning to occur within a typical cloud lifetime. Weak clouds, i.e. those with a small value of a_1, have $|\sigma_i| = |\sigma_r|$ at L = 2 π v τ which can be considered as being equivalent to the charging length limit l_c. For increasing cloud strength a simple cloud structure is allowed for decreasing length scales, in agreement with the numerical slab model experiments in Appendix 1, as shown by a comparison of Figures A.5 and A.12.

This analysis indicates how oscillatory charge structures can occur in the inductive effect, and not just the simple dipole, even in infinite clouds providing that the electrical forcing is weak. The effect of the cloud aspect ratio, through a finite α , is expected to increase this tendency. The extremely simplified nature of the basic assumptions in this case suggests that a more detailed examination of the given derivation will be of doubtful validity.

APPENDIX FIGURE CAPTIONS

Fig. A.1 Charge distributions Q^c, Q^p (C) and electric field E (kVm^{-1}) variation with height z (km) in the charging zone of a narrow cloud at t = 30 minutes for the slab model. The cloud parameters are those for the default case except that the cloud radius , R = 1.0 km.

Fig. A.2 As in (A.1) , except that t = 25 minutes and R = 2.0 km.

Fig. A.3 As in (A.1) , except that t = 20 minutes and R = 4.0 km.

Fig. A.4 The maximum electric field in kVm^{-1} as a function of time in minutesfor the slab model. The values of N refer to the number of gridpoints describing the vertical dimension, which is of constant total height 14 km.

Fig.A.5 As in (A.4) for the default parameters with differing cloud radii R in km. The figures plotted on the growth curves give the number of reversals of electric field direction within the charging zone.

Fig. A.6 As in (A.4) for the default case with different time integration periods .

Fig. A.7 As in (A.4) for different advection schemes. The full line is the simple upsteam; the dashed line is the upsream finite element; the dot-dash line is the centred difference method.

Fig. A.8 As in (A.5) for the 'broad' charging zone sec^{-1} (z in km).

Fig. A.9 As in (A.8) for the'sharp' charging zone sec^{-1} (z in km).

Fig. A.10 As in (A.5) for the 'weak' charging zone sec^{-1} (z in km).

Fig. A.11 As in (A.4) for different fallspeeds v in ms^{-1}.

Fig. A.12 As in (A.5) for the weak electrical forcing given by $a_1 = 10^{-14}$ (m.k.s. units).

Fig. A.13 The dependence on the vertical length scale $L = 2\pi/k$ of the modulus of the real and imaginary parts of the frequency $\sigma = \sigma_r + i\sigma_i$ (sec^{-1}) for allowed modes of growth. The wave disturbance is then of the form $\exp i(kz + \sigma_r t) \cdot \exp|\sigma_i| t$.

Fig. A.14 The full line describes the threshold length scale L for which $|\sigma_r| = |\sigma_i|$ versus the electrical forcing; the region above this line allows simple growth. The dashed line describes the limit for which $|\sigma_i| = 6.10^{-3}$ sec^{-1}; the region above this line allows sufficient growth for lightning to occur within the lifetime of a cloud.

FIGURE 1

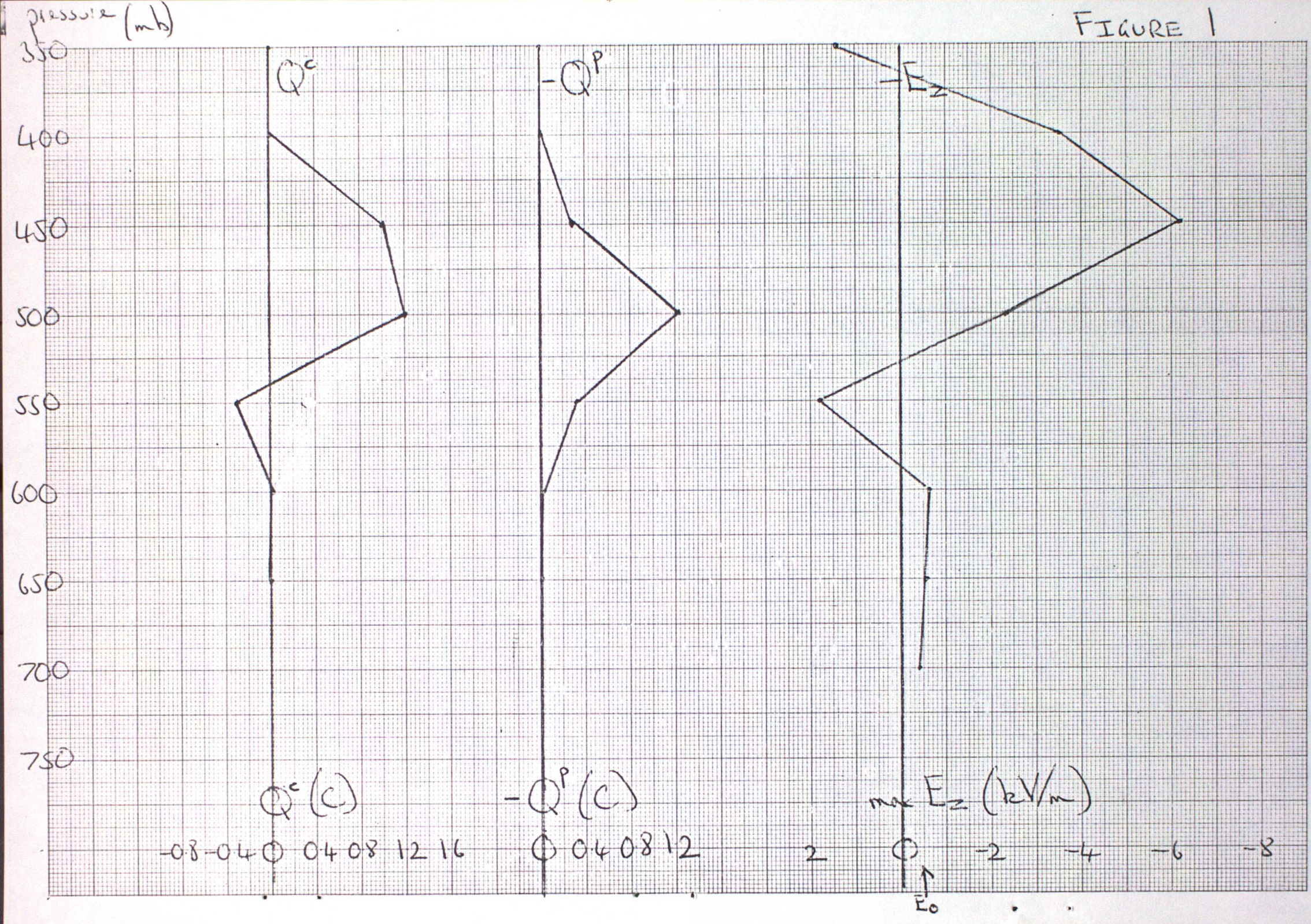
pression (mb)
350
400
450
500
550
600
650
700
750
Q^c
$-Q^p$
E_z
Q^c (C)
-08 -04 0 04 08 12 16
$-Q^p$ (C)
0 04 08 12
max E_z (kV/m)
2 0 -2 -4 -6 -8
E_0

FIGURE 2

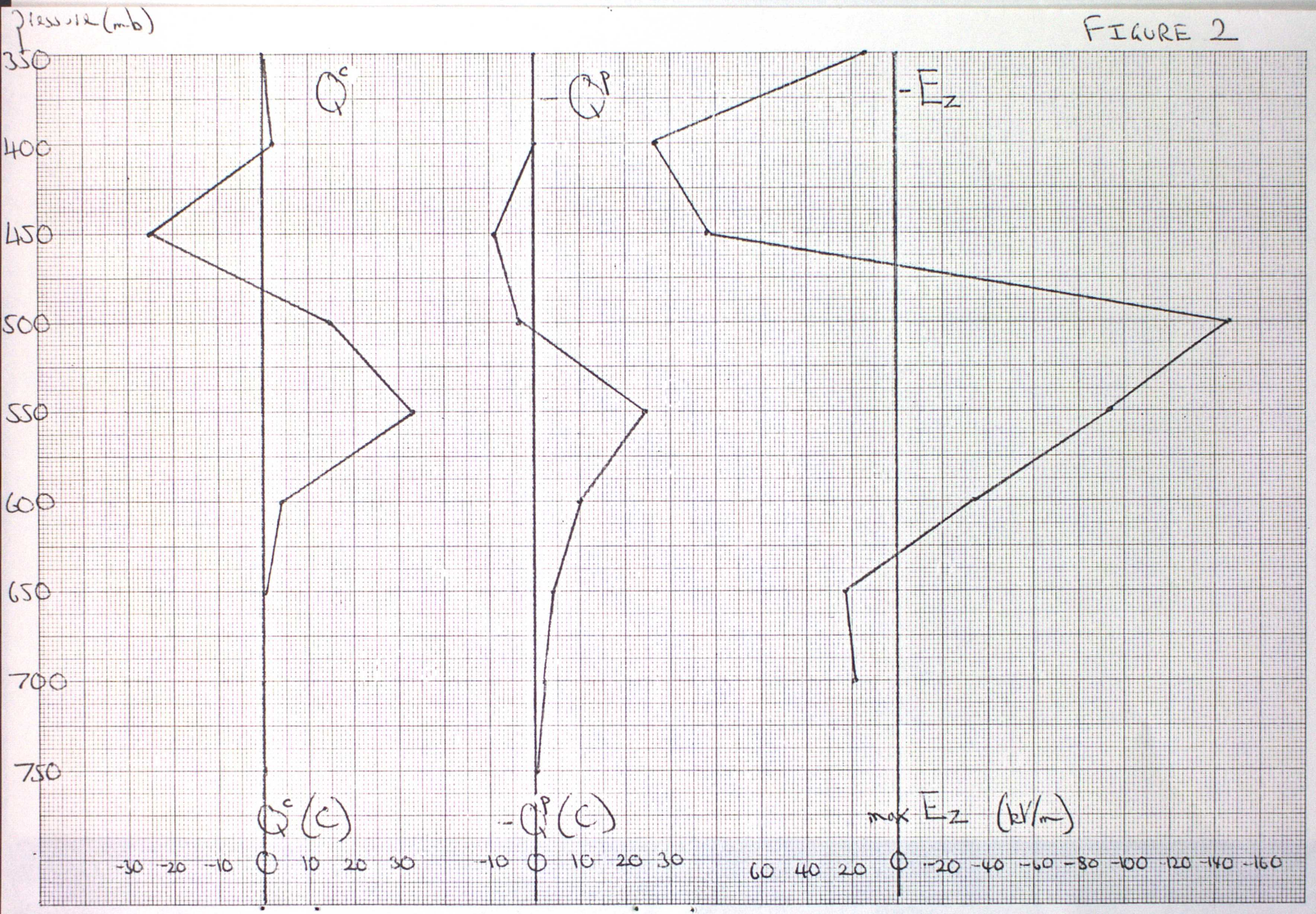
Pressure (mb)
350
400
450
500
550
600
650
700
750
Q^c
$-Q^p$
$-E_z$
Q^c (C)
$-Q^p$ (C)
max E_z (kV/m)
-30 -20 -10 0 10 20 30
-10 0 10 20 30
60 40 20 0 -20 -40 -60 -80 -100 -120 -140 -160

FIGURE 3

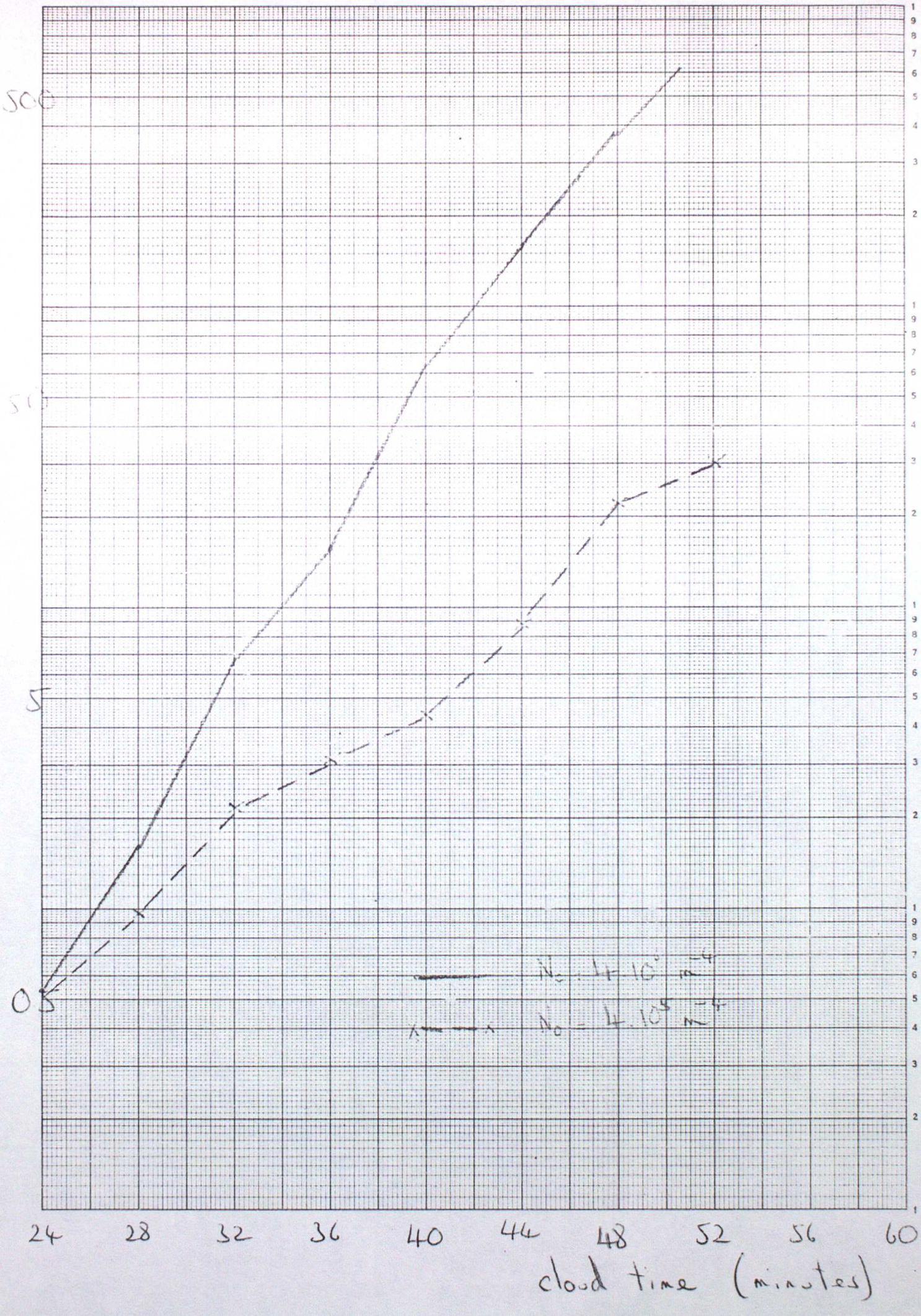
E. max field (kV/m)
500
50
5
0.5
24
28
32
36
40
44
48
52
56
60
cloud time (minutes)
$N_0 = 4 \times 10^4\ m^{-4}$
$N_0 = 4 \times 10^5\ m^{-4}$
Log 4 Cycles x mm, ½ and 1 cm
Graph Data Ref. 5541
Chartwell

FIGURE 4

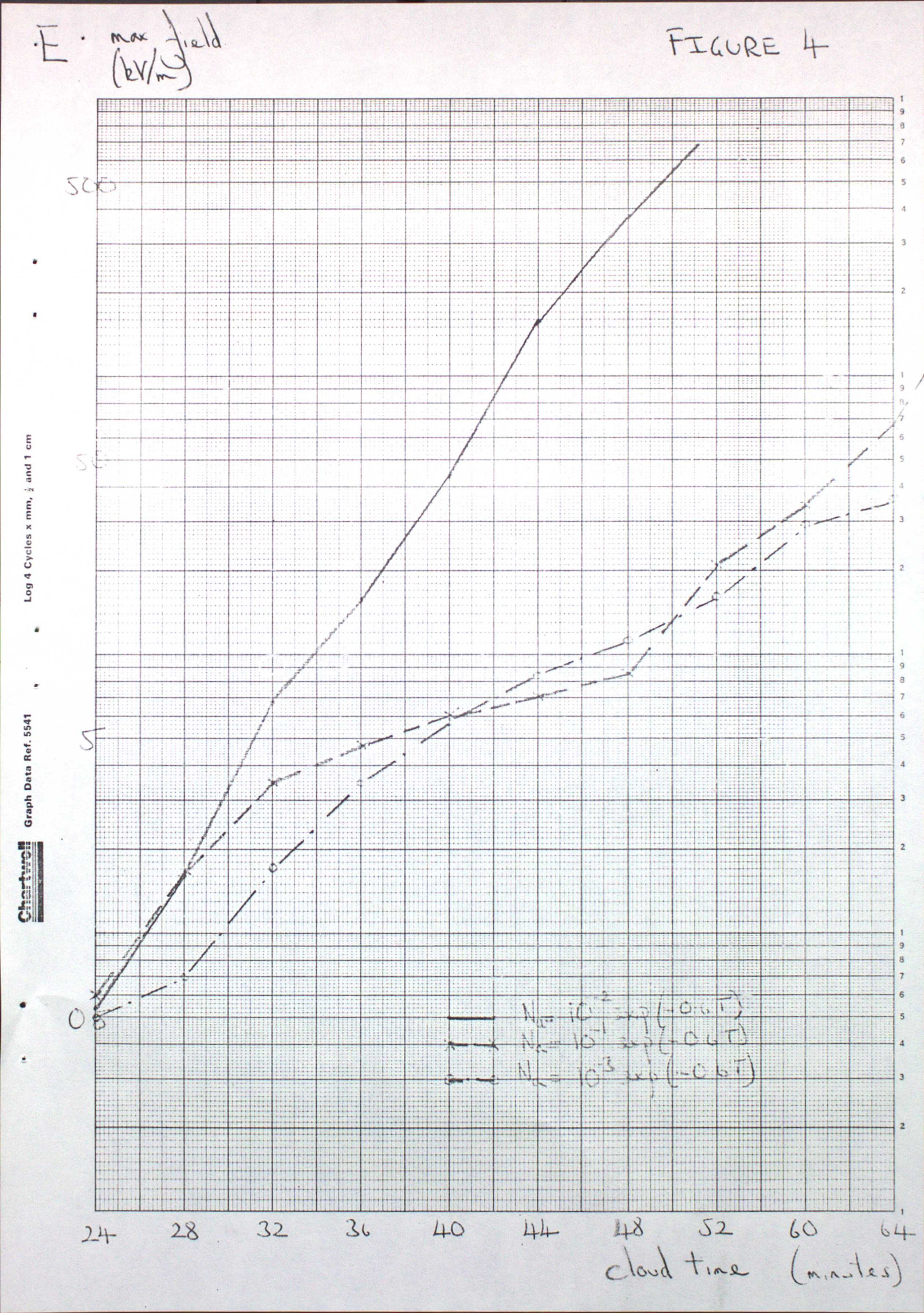
E · max field (kV/m)
500
50
5
0
24
28
32
36
40
44
48
52
60
64
cloud time (minutes)
Log 4 Cycles x mm, ½ and 1 cm
Graph Data Ref. 5541
Chartwell

FIGURE 5

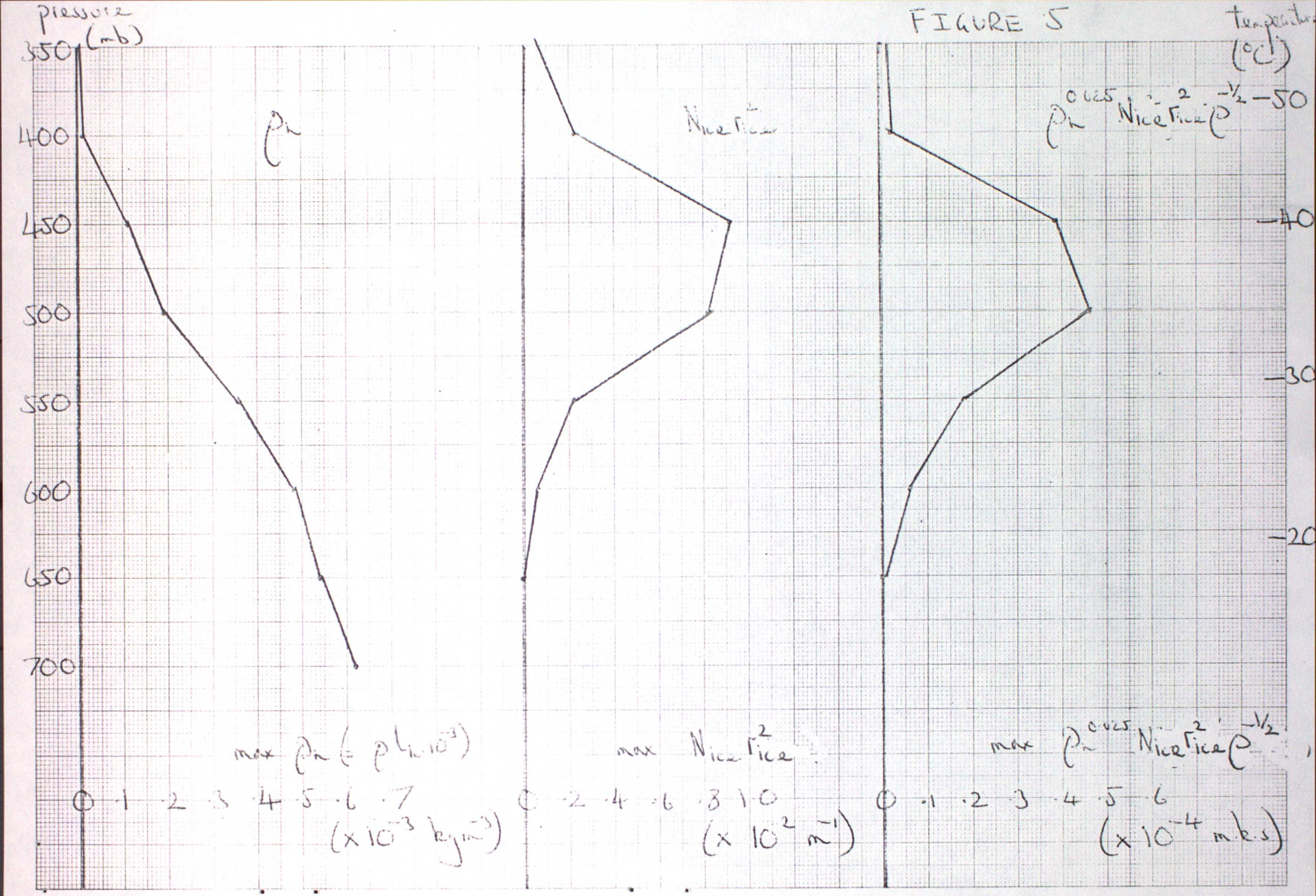
pressure (mb)
temperature (°C)
350
400
450
500
550
600
650
700
−50
−40
−30
−20
ρ_a
$N_{ice}\Gamma_{ice}^2$
$\rho_a^{0.625} N_{ice}\Gamma_{ice}^2 \rho^{-1/2}$
max ρ_a (= $\rho_a \cdot 10^3$)
0 1 2 3 4 5 6 7
($\times 10^{-3}$ kg m^{-3})
max $N_{ice}\Gamma_{ice}^2$
0 2 4 6 8 10
($\times 10^2$ m^{-1})
max $\rho_a^{0.625} N_{ice}\Gamma_{ice}^2 \rho^{-1/2}$
0 1 2 3 4 5 6
($\times 10^{-4}$ m.k.s)

FIGURE 6

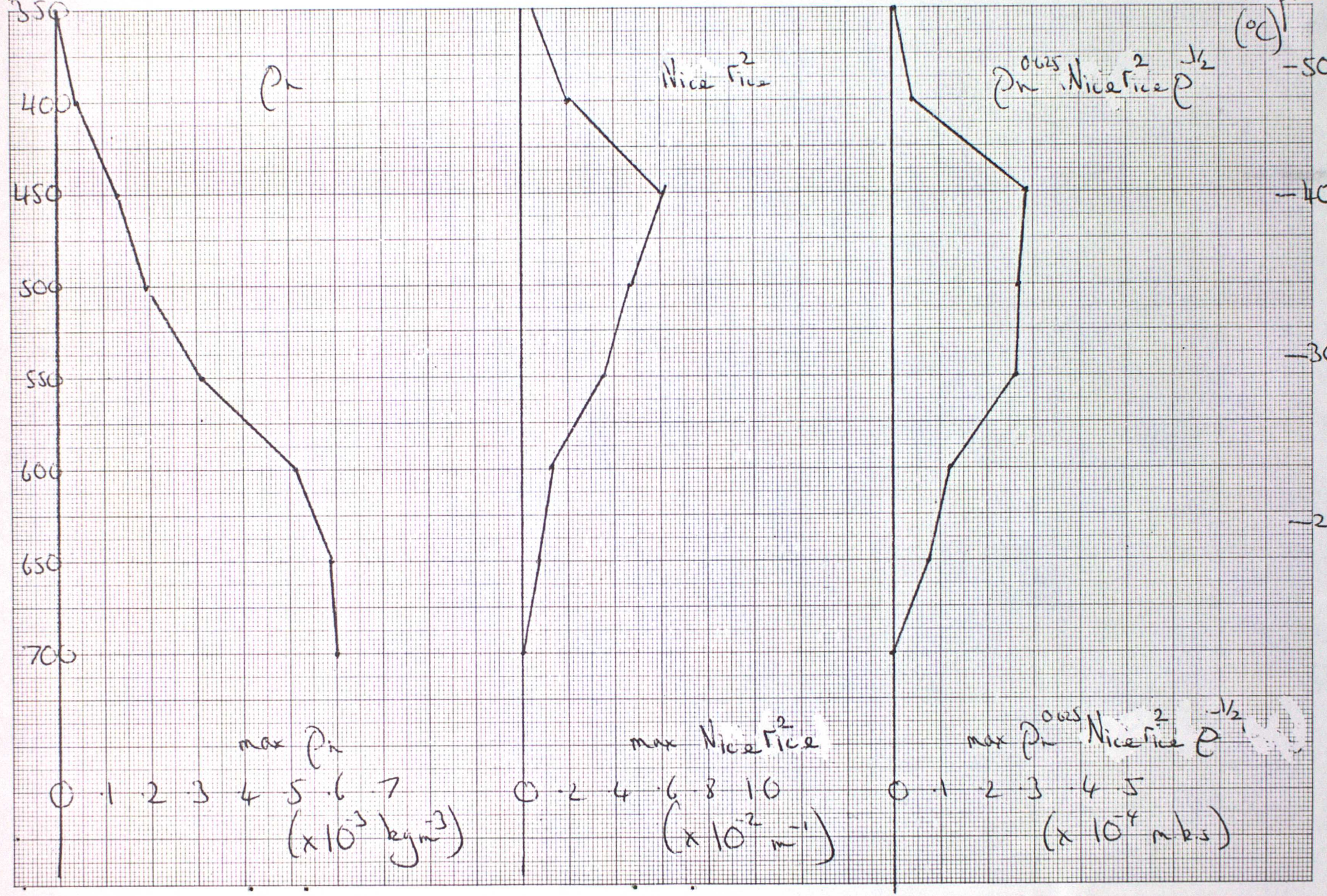
pressure (mb)
350
400
450
500
550
600
650
700
ρ_x
max ρ_x
0 1 2 3 4 5 6 7
($\times 10^{-3}$ kg m^{-3})
$N_{ice} r_{ice}^2$
max $N_{ice} r_{ice}^2$
0 2 4 6 8 10
($\times 10^{-2}$ m^{-1})
$\rho_x^{0.625} N_{ice} r_{ice}^2 \rho^{-1/2}$
max $\rho_x^{0.625} N_{ice} r_{ice}^2 \rho^{-1/2}$
0 1 2 3 4 5
($\times 10^{-4}$ m$^{1.5}$)
temperature (°C)
-50
-40
-30
-20

FIGURE 7

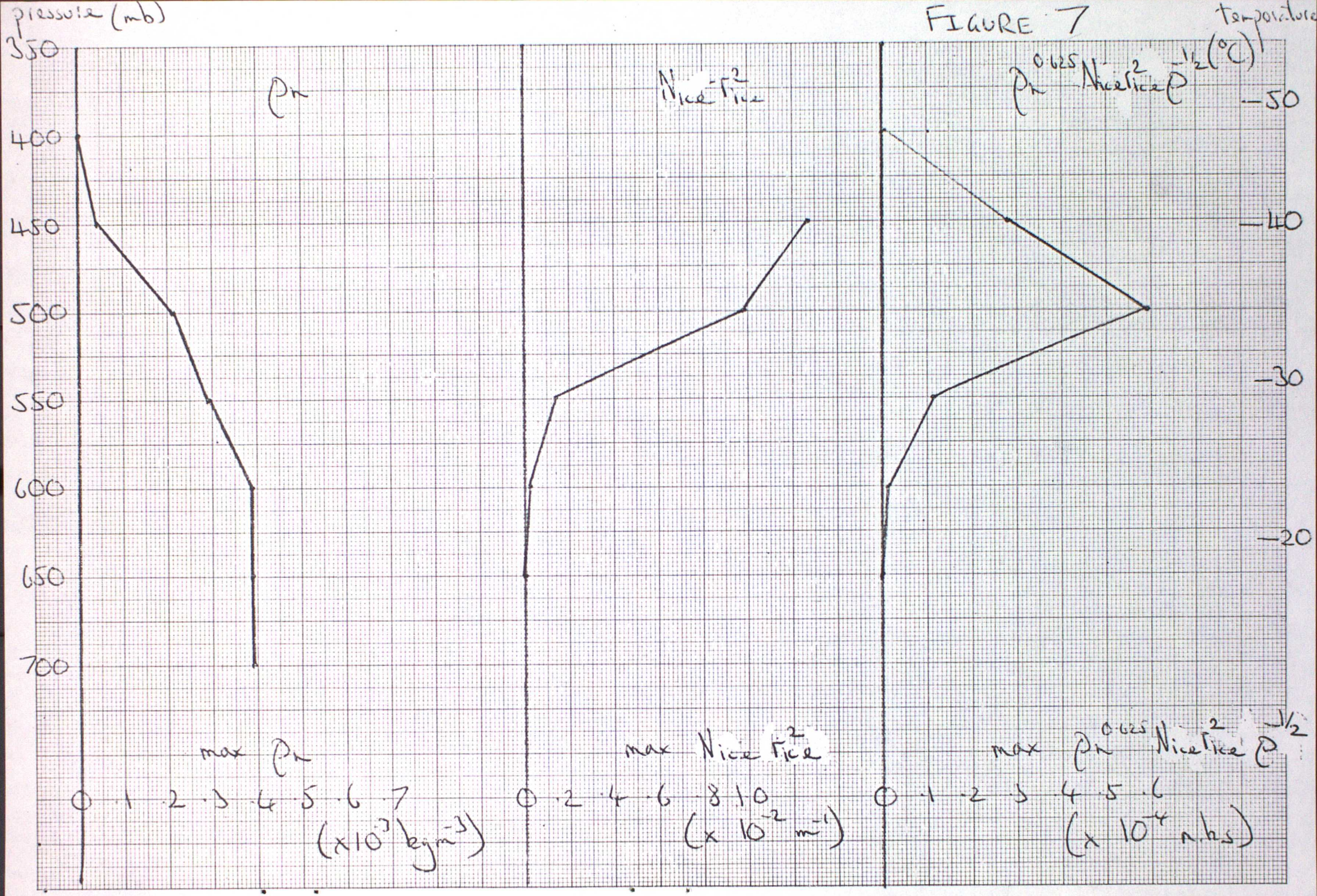
pressure (mb)
350
400
450
500
550
600
650
700
ρ_r
max ρ_r
0 1 2 3 4 5 6 7
($\times 10^{-3}$ kg m^{-3})
$N_{ice} r_{ice}^2$
max $N_{ice} r_{ice}^2$
0 2 4 6 8 10
($\times 10^{-2}$ m^{-1})
$\rho_r^{0.625} N_{ice} r_{ice}^2 \rho^{-1/2}$
max $\rho_r^{0.625} N_{ice} r_{ice}^2 \rho^{-1/2}$
0 1 2 3 4 5 6
($\times 10^{-4}$ m.h.s)
temperature (°C)
−50
−40
−30
−20
−1/2

t = 30 mins R = 1 km

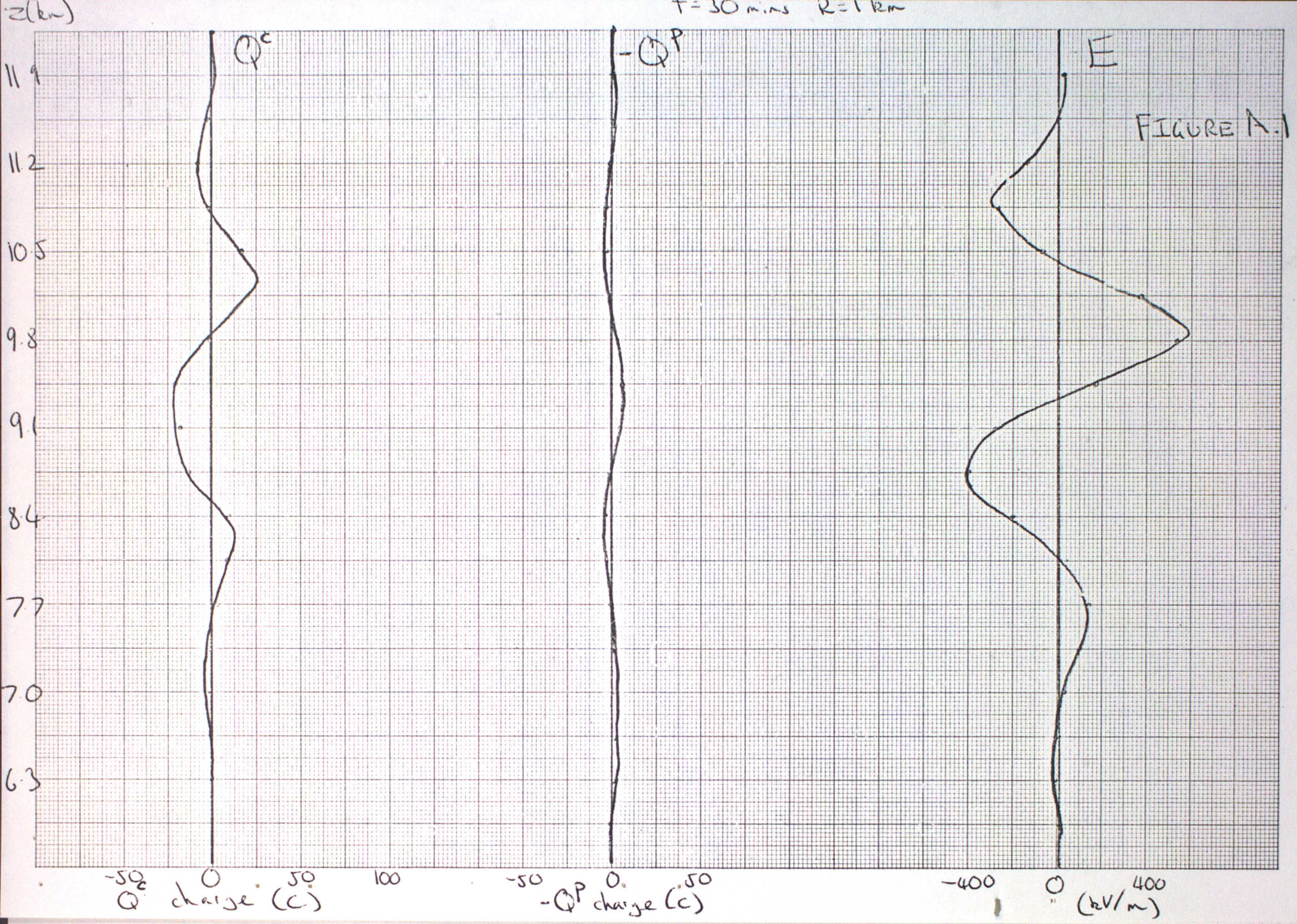

FIGURE A.1

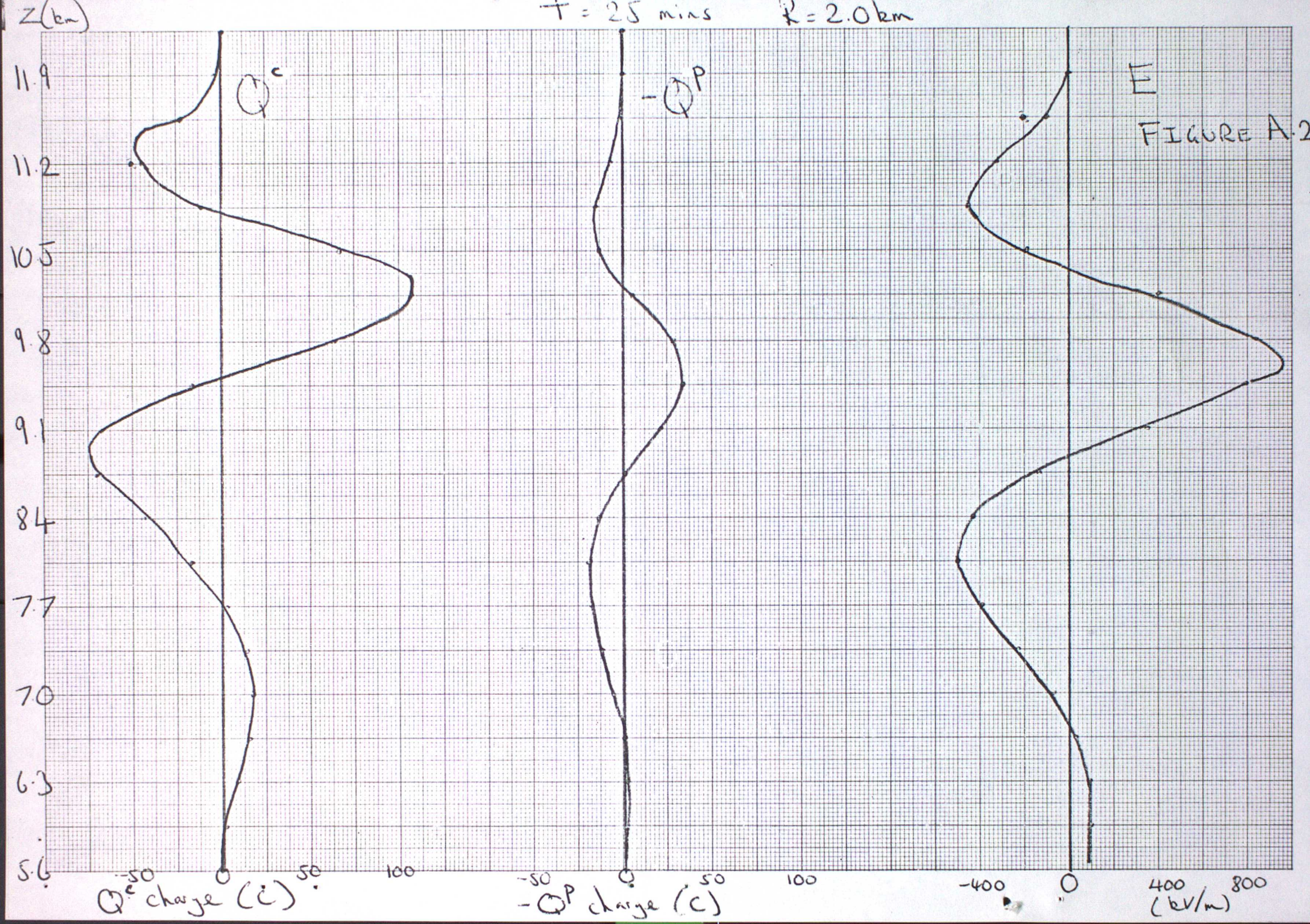
T = 25 mins
R = 2.0 km
Z (km)
11.9
11.2
10.5
9.8
9.1
8.4
7.7
7.0
6.3
5.6
Q^c
$-Q^P$
E
-50
0
50
100
Q^c charge (C)
-50
0
50
100
$-Q^P$ charge (C)
-400
0
400
800
(kV/m)

FIGURE A.2

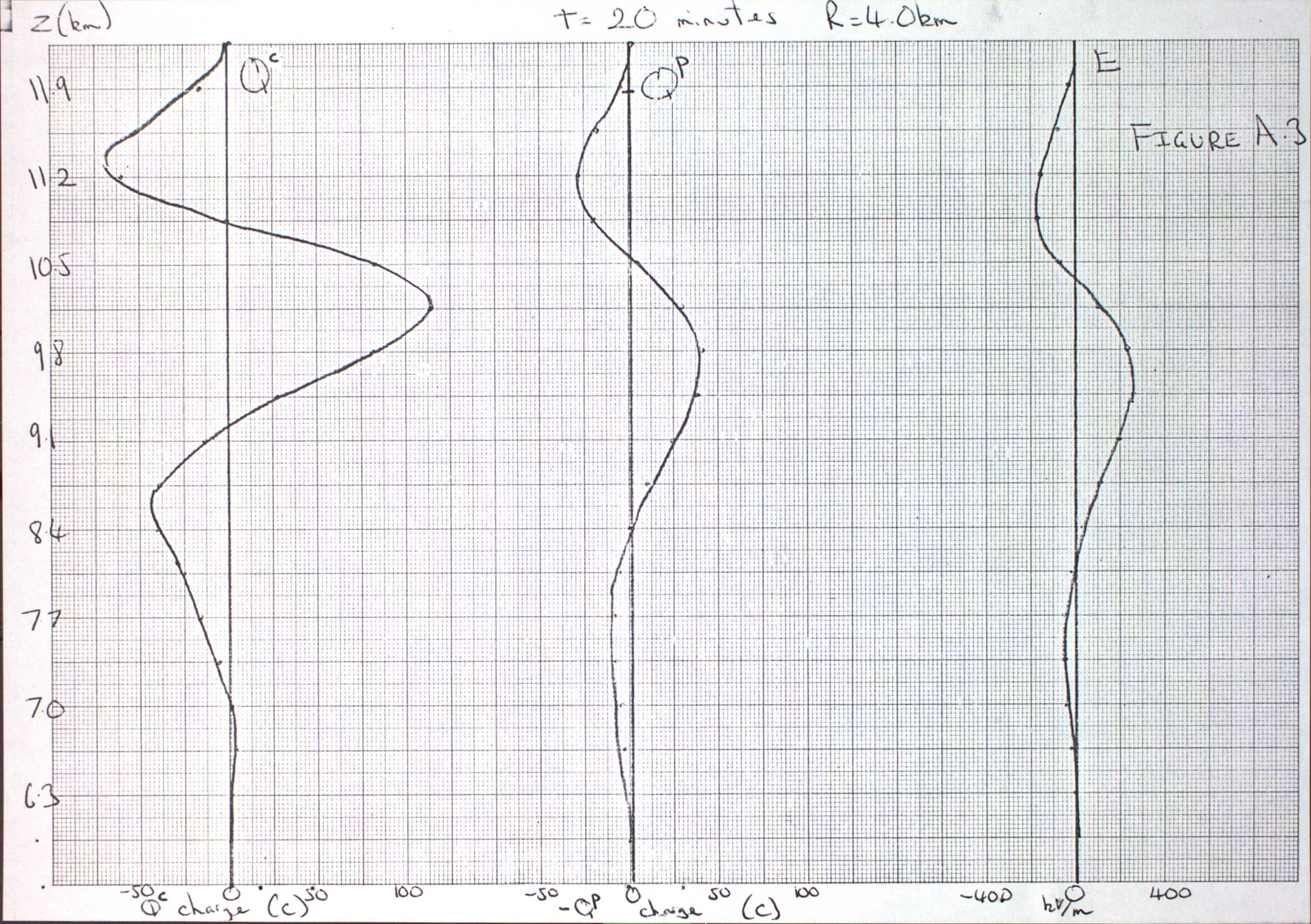
z (km)
t = 20 minutes R = 4.0km
11.9
11.2
10.5
9.8
9.1
8.4
7.7
7.0
6.3
Q^c
Q^p
E
-50
Q^c charge (c)
50
100
-50
$-Q^p$
charge
50
(c)
100
-400
kV/m
400

FIGURE A.3

max electric field (kV/m)

NUMERICAL SLAB MODEL

FIGURE A.4

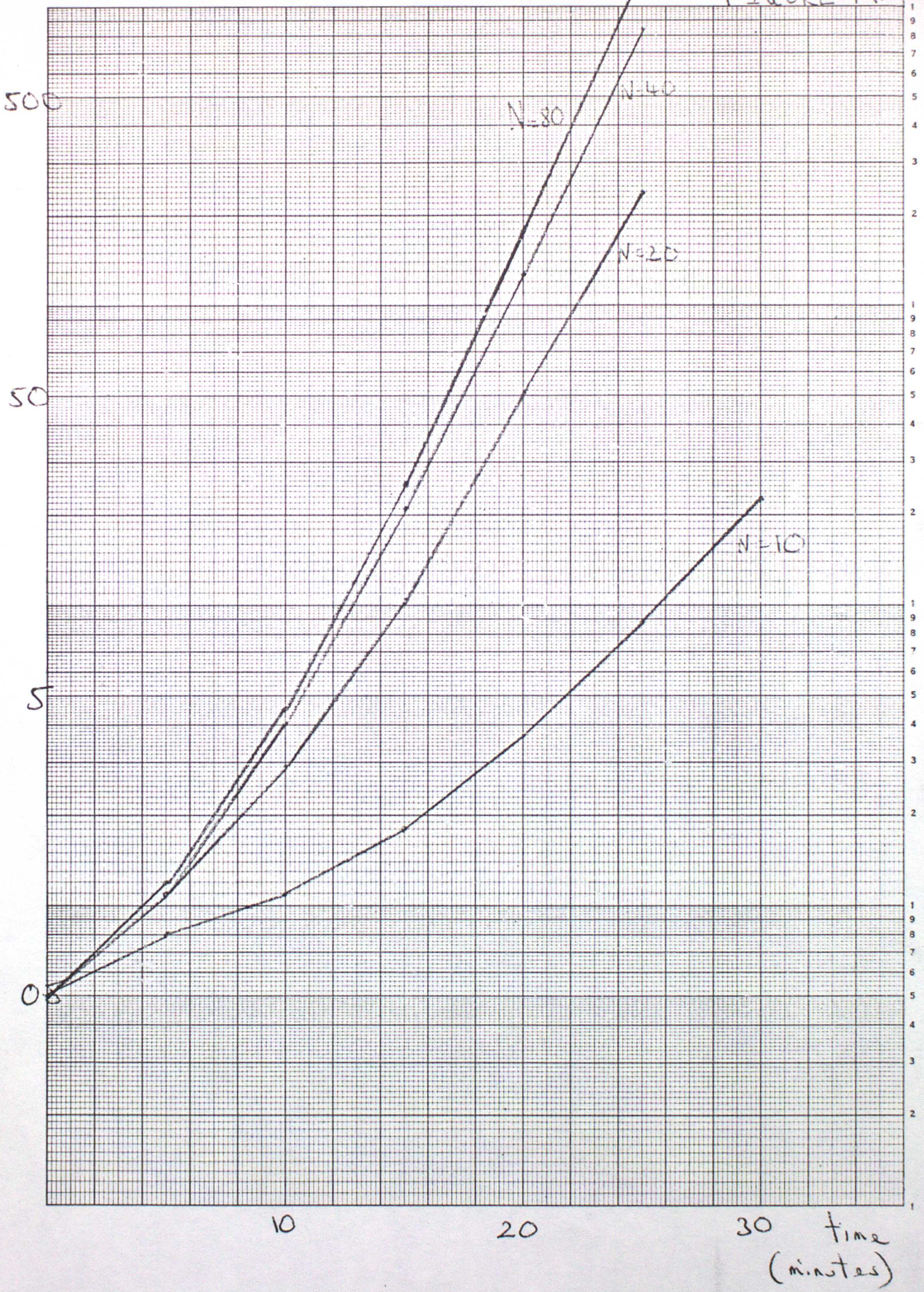

max. electric field (kV/m)

NUMERICAL SLAB MODEL

FIGURE A.5

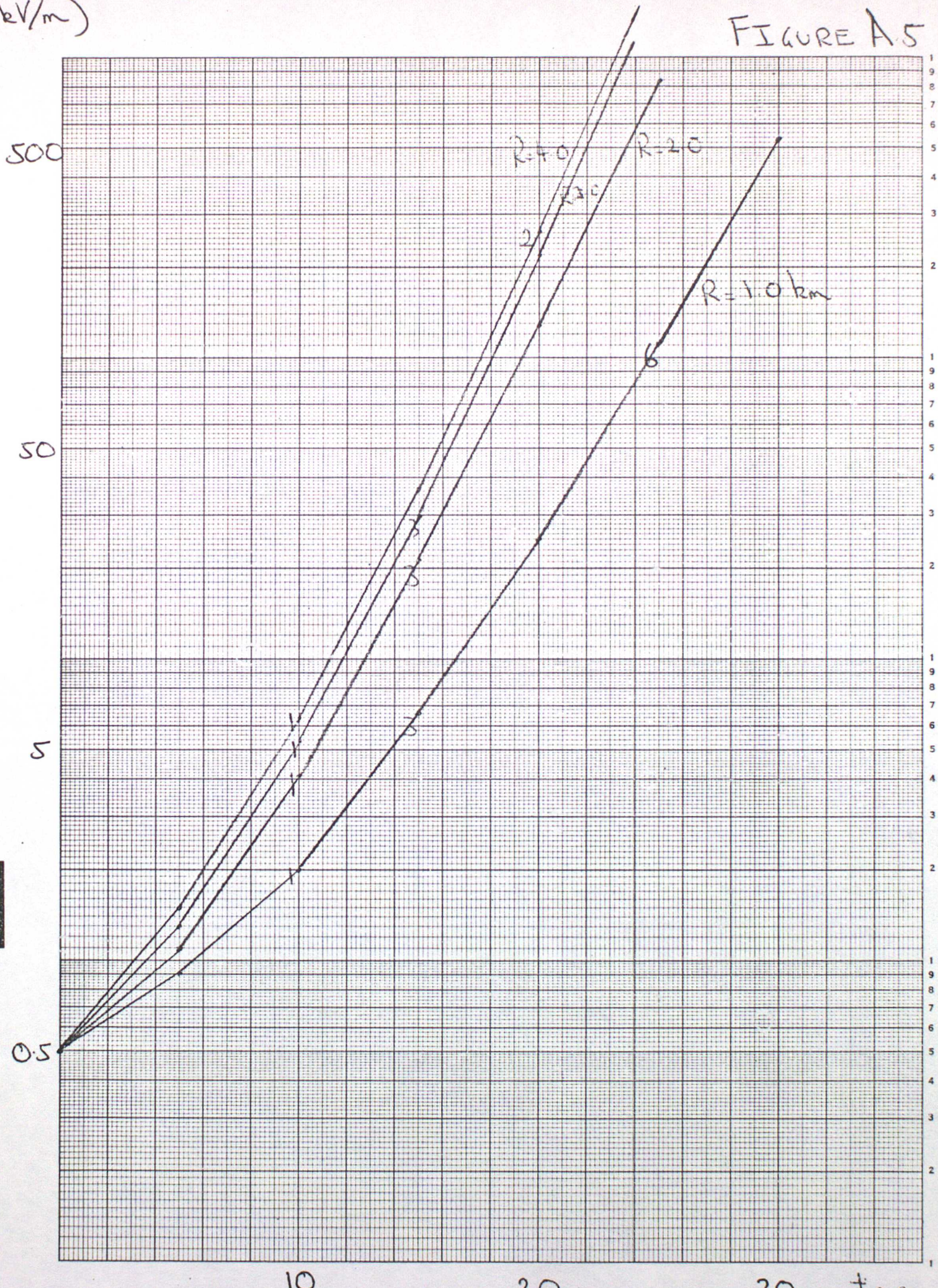

NUMERICAL SLAB MODEL

FIGURE A.6

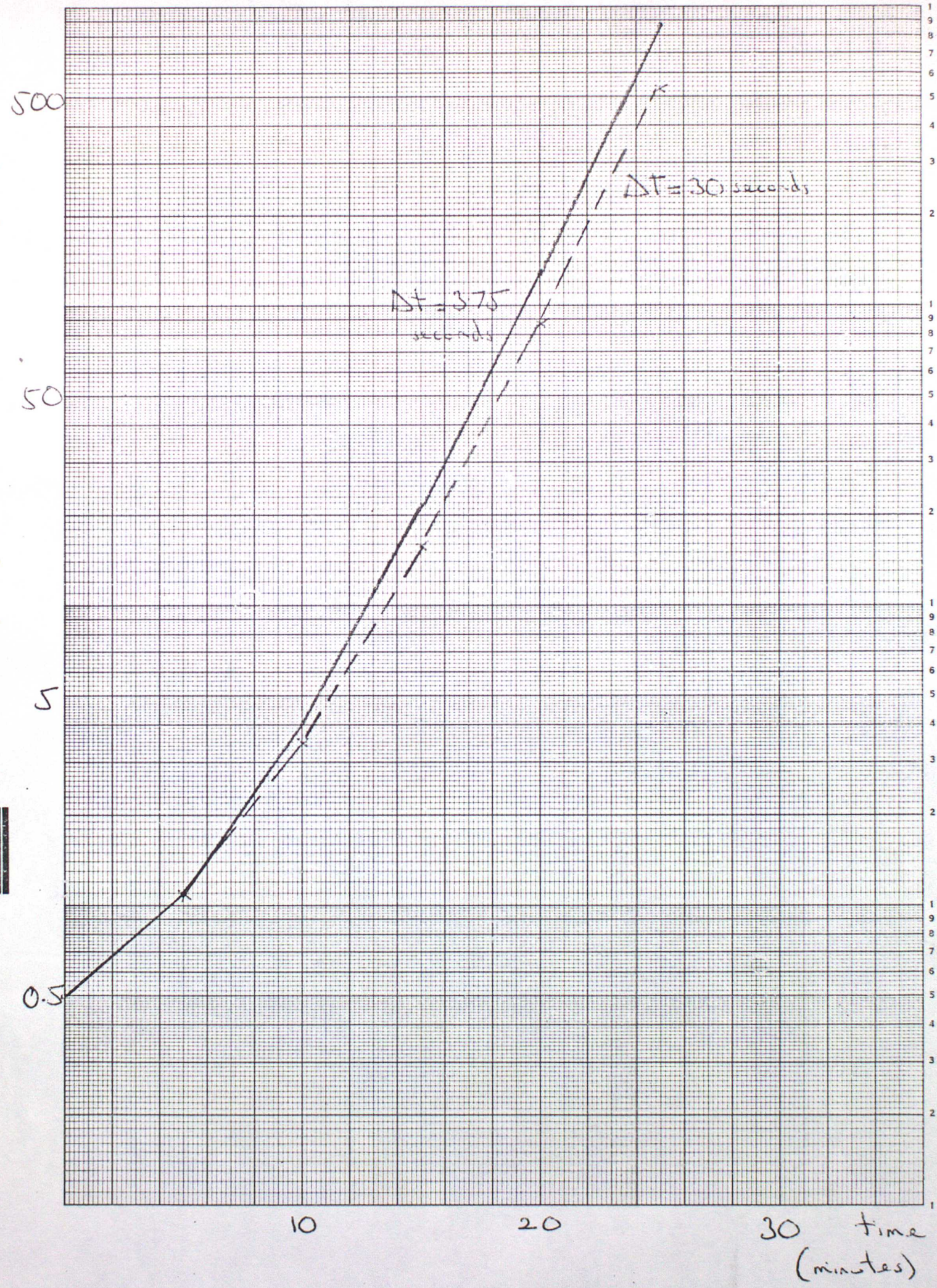

max electric field (kV/m)

NUMERICAL SLAB MODEL

FIGURE A.7

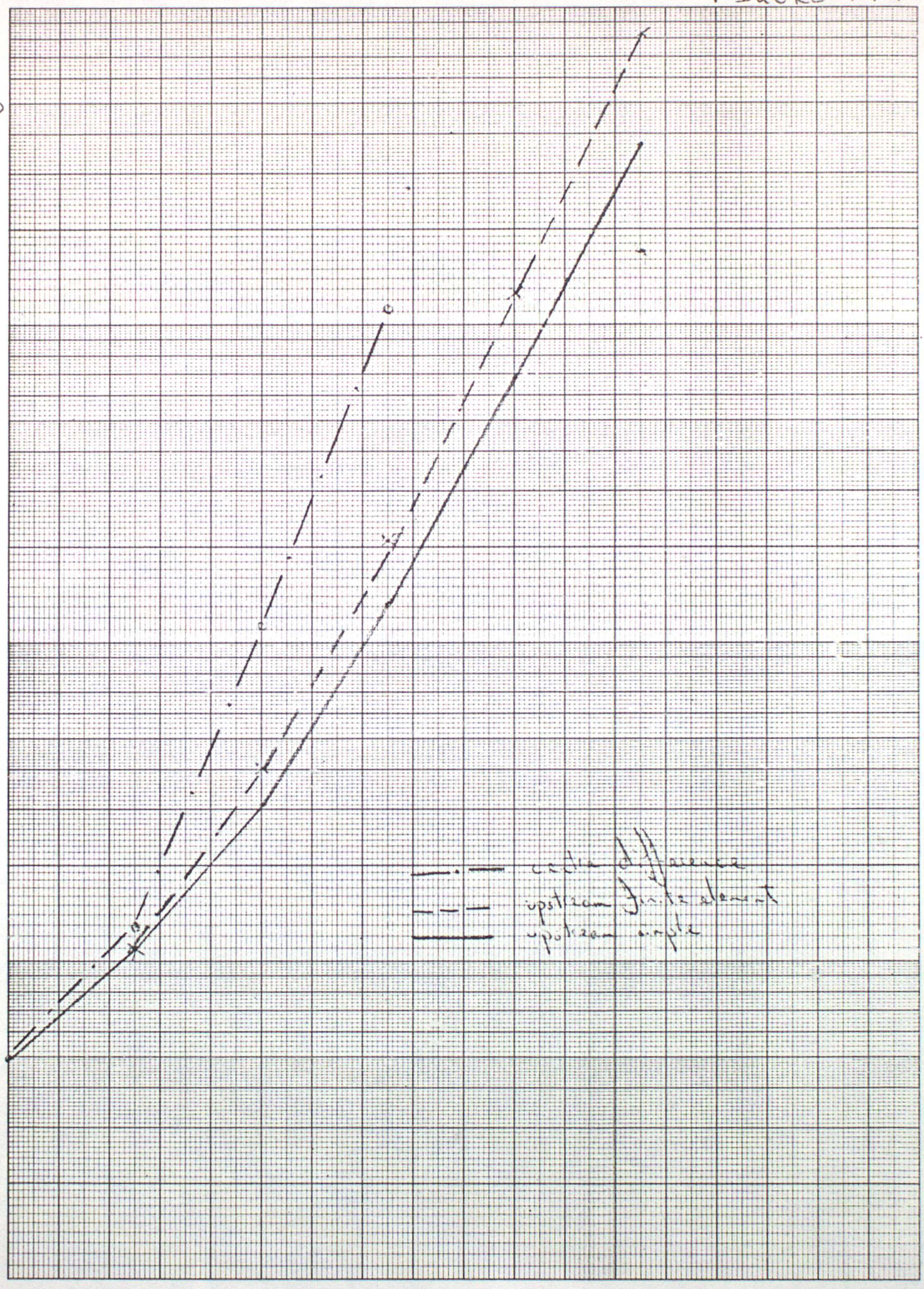

max. electric field (kV/m)

NUMERICAL SLAB MODEL

FIGURE A.8

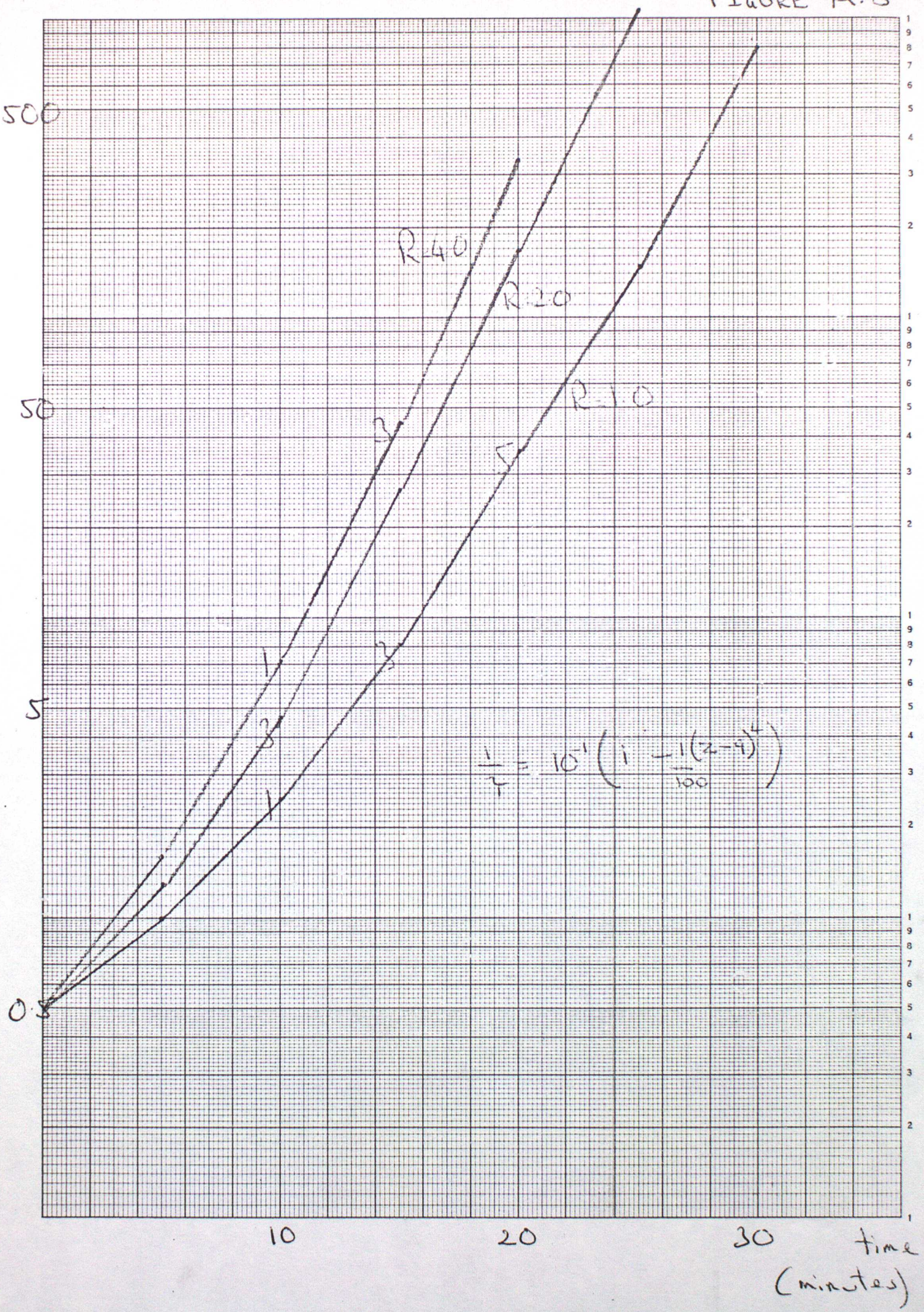

Log 4 Cycles x mm, ½ and 1 cm

Graph Data Ref. 5541

Chartwell

max. electric field (kV/m)

NUMERICAL SLAB MODEL

FIGURE A.9

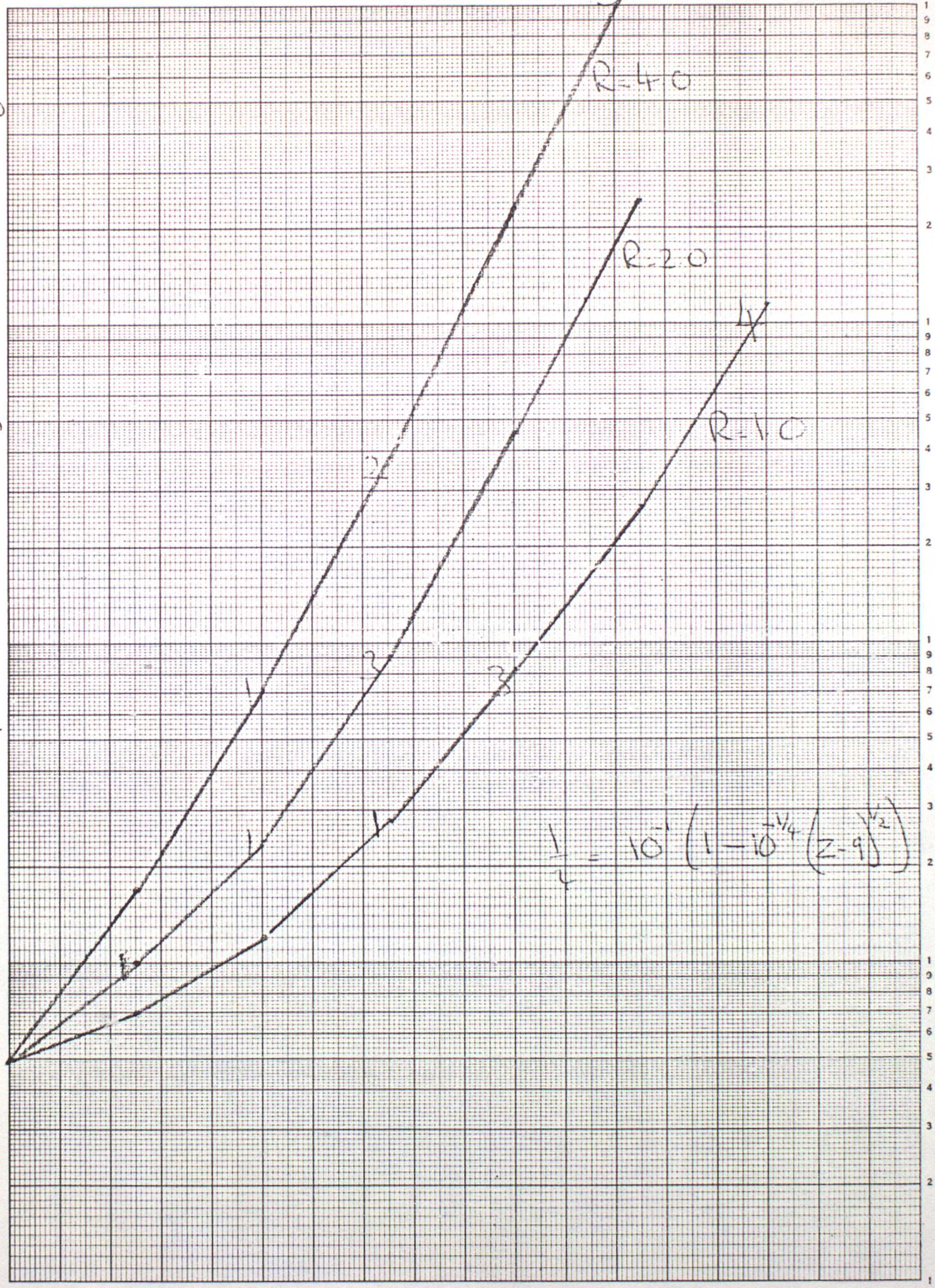

Log 4 Cycles x mm, ½ and 1 cm

Graph Data Ref. 5541

Chartwell

max. electric field (kV/m)

NUMERICAL SLAB MODEL

FIGURE A.10

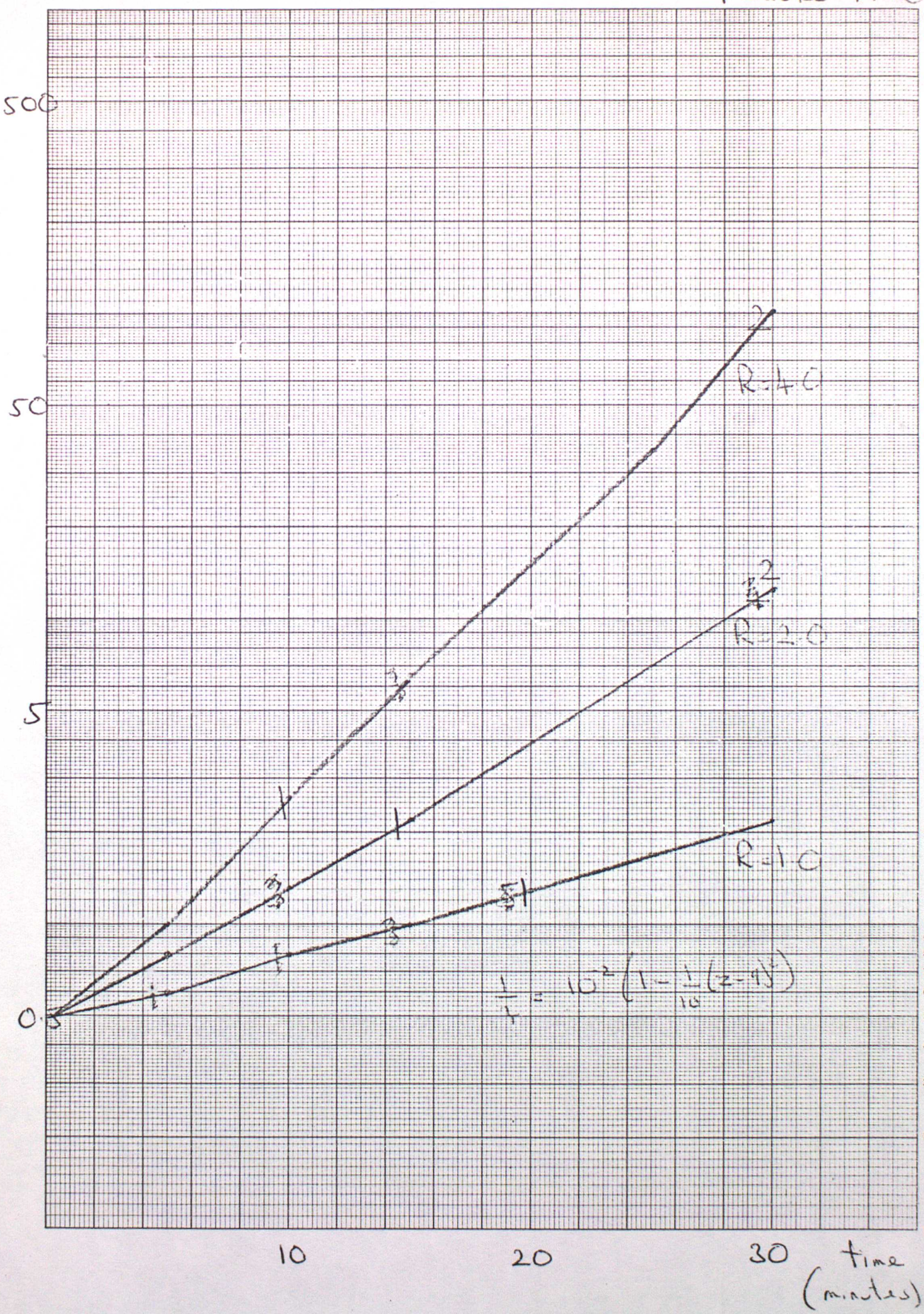

max electric field (kV/m)

NUMERICAL SLAB MODEL

FIGURE A.11

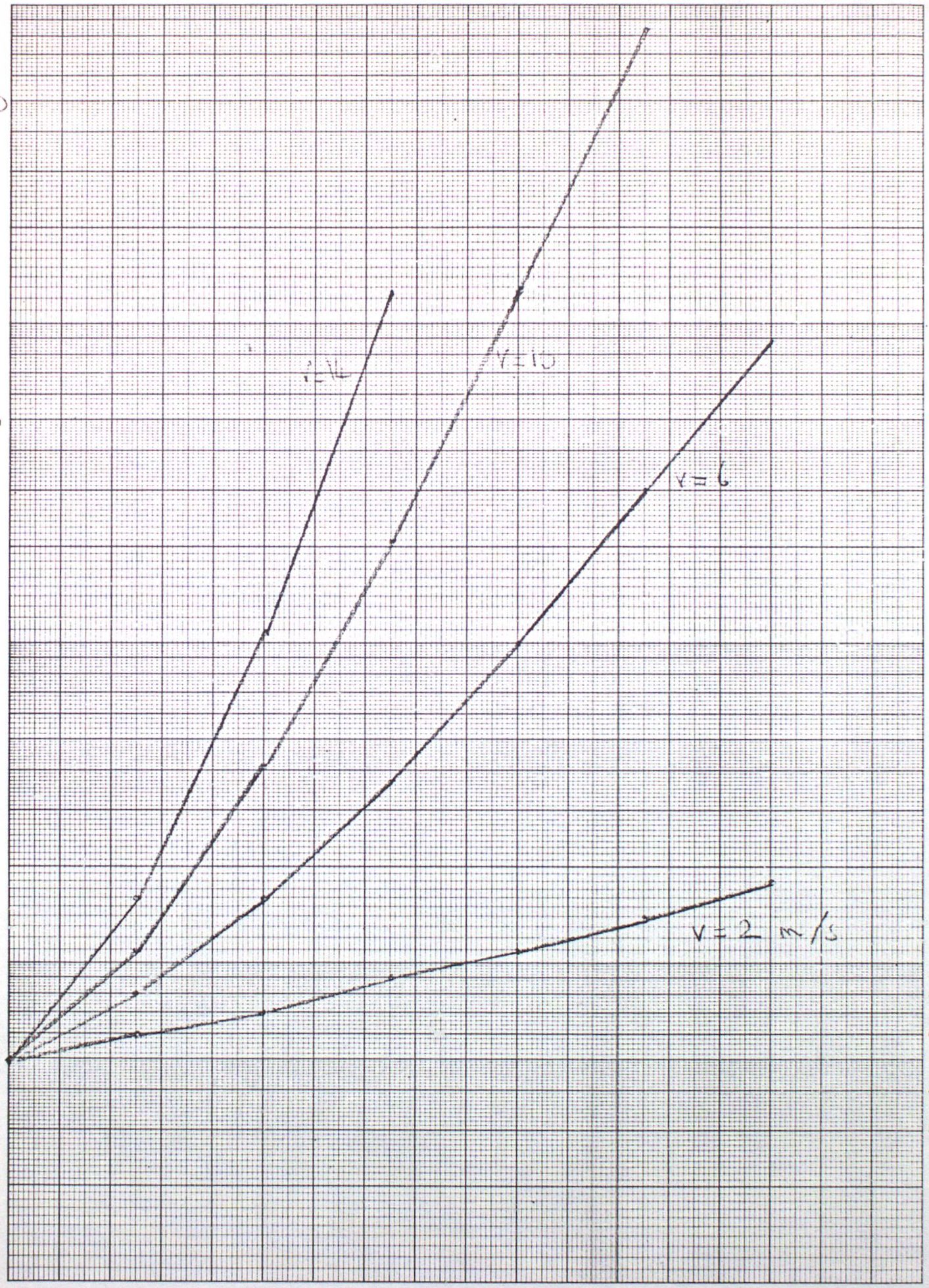

Log 4 Cycles x mm, ½ and 1 cm

Graph Data Ref. 5541

Chartwell

max electic field (kV/m)

NUMERICAL SLAB MODEL

FIGURE A·12

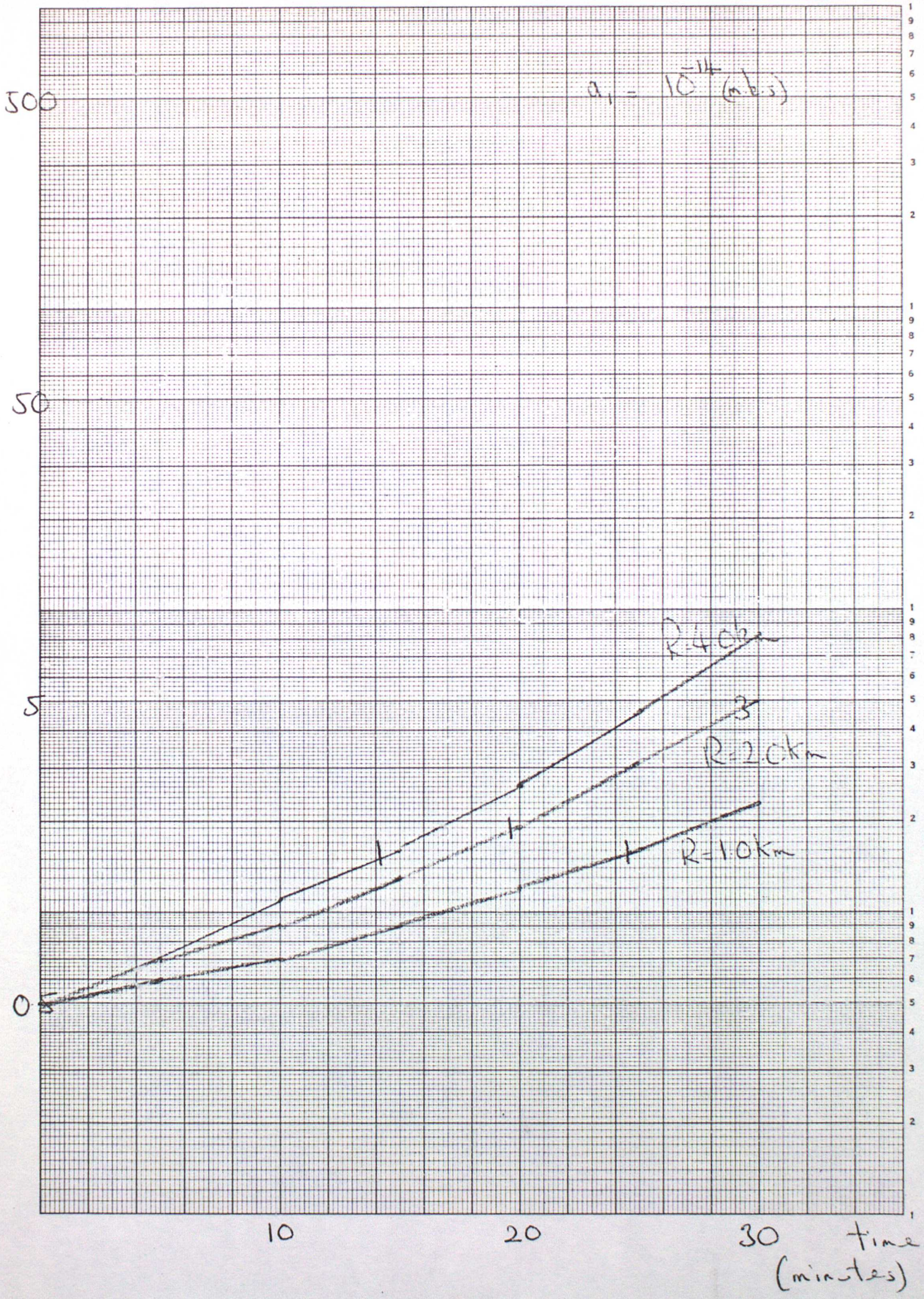

1-D MODEL

L vertical length scale

FIGURE A.13

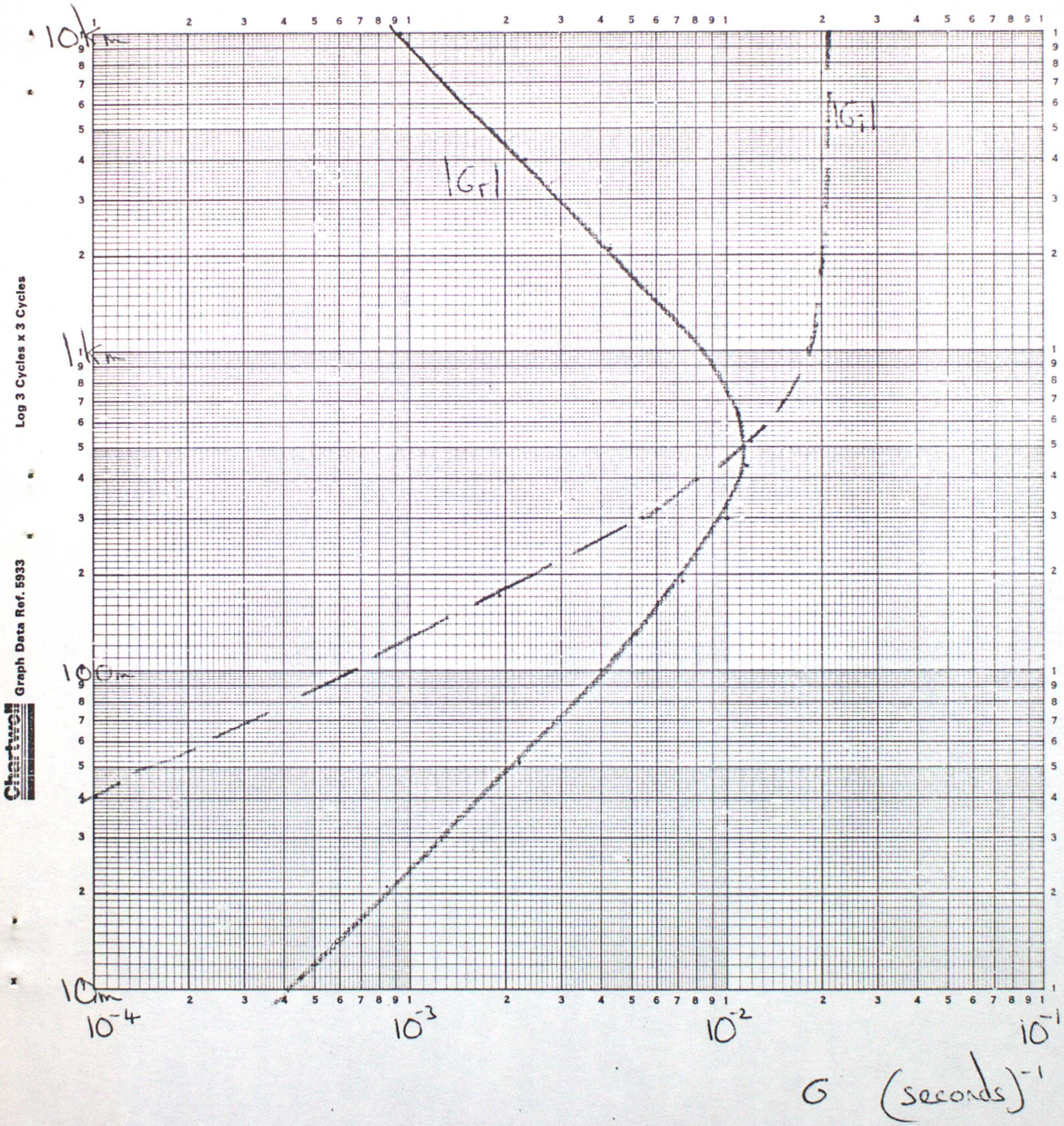

1-D MODEL

L vertical length scale

FIGURE A.14

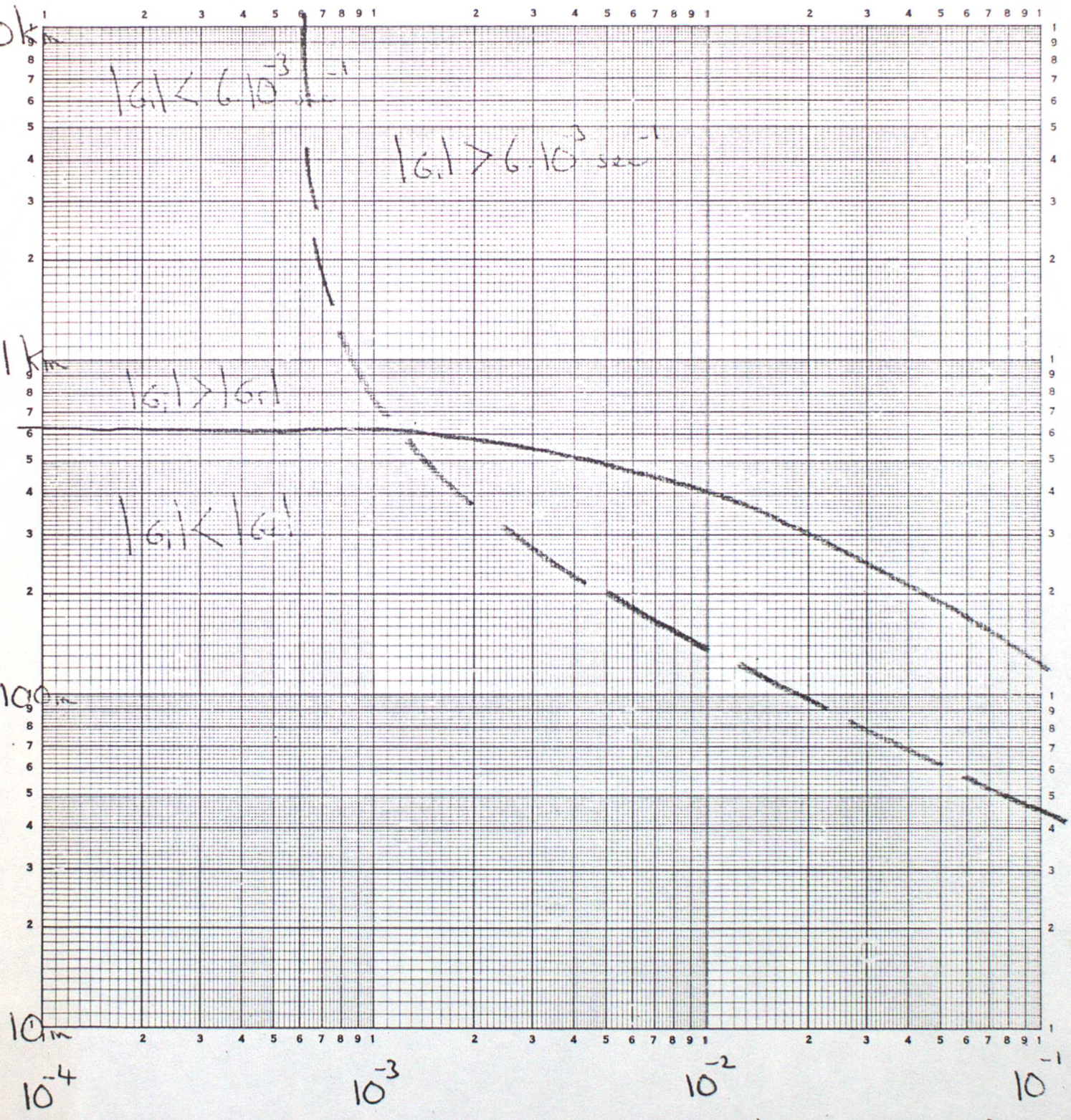

Log 3 Cycles x 3 Cycles

Chartpac Graph Data Ref. 5933